Article

Psilocybin's lasting action requires pyramidal cell types and 5-HT$_{2A}$ receptors

https://doi.org/10.1038/s41586-025-08813-6

Received: 5 August 2023

Accepted: 19 February 2025

Published online: 2 April 2025

Check for updates

Ling-Xiao Shao[1,2,7], Clara Liao[1,3,7], Pasha A. Davoudian[1,3,4], Neil K. Savalia[1,3,4], Quan Jiang[1], Cassandra Wojtasiewicz[1], Diran Tan[1], Jack D. Nothnagel[1], Rong-Jian Liu[2], Samuel C. Woodburn[1], Olesia M. Bilash[1], Hail Kim[5], Alicia Che[2] & Alex C. Kwan[1,2,6]✉

Psilocybin is a serotonergic psychedelic with therapeutic potential for treating mental illnesses[1–4]. At the cellular level, psychedelics induce structural neural plasticity[5,6], exemplified by the drug-evoked growth and remodelling of dendritic spines in cortical pyramidal cells[7–9]. A key question is how these cellular modifications map onto cell-type-specific circuits to produce the psychedelics' behavioural actions[10]. Here we use in vivo optical imaging, chemogenetic perturbation and cell-type-specific electrophysiology to investigate the impact of psilocybin on the two main types of pyramidal cells in the mouse medial frontal cortex. We find that a single dose of psilocybin increases the density of dendritic spines in both the subcortical-projecting, pyramidal tract (PT) and intratelencephalic (IT) cell types. Behaviourally, silencing the PT neurons eliminates psilocybin's ability to ameliorate stress-related phenotypes, whereas silencing IT neurons has no detectable effect. In PT neurons only, psilocybin boosts synaptic calcium transients and elevates firing rates acutely after administration. Targeted knockout of 5-HT$_{2A}$ receptors abolishes psilocybin's effects on stress-related behaviour and structural plasticity. Collectively, these results identify that a pyramidal cell type and the 5-HT$_{2A}$ receptor in the medial frontal cortex have essential roles in psilocybin's long-term drug action.

Psilocybin is a classic psychedelic that has shown promise as a treatment for psychiatric disorders. Clinical trials demonstrated that one or two sessions of psilocybin-assisted therapy attenuate depression symptoms for many weeks[1–3]. It has been hypothesized that antidepressants may work by forming and strengthening synapses in the prefrontal cortex, which counteracts synaptic dysfunction in depression[11]. Consistent with this framework, recent studies in mice demonstrated that a single dose of psilocybin or related psychedelic drugs leads to sustained increases in the density and size of apical dendritic spines in cortical pyramidal cells[7–9,12,13].

However, neurons are heterogeneous, and it is unclear how psychedelic-evoked neural adaptations manifest in different excitatory cell types. Notably, there are two major, non-overlapping populations of cortical pyramidal cells—PT and IT neurons. PT and IT neurons have distinct cellular properties and participate in different long-range circuits because they send disparate axonal projections to communicate with different brain regions[14–16] (Fig. 1a). PT neurons are predominantly subcerebral projection neurons that send axons to subcortical destinations, including the thalamus and brainstem[16]. By contrast, axons of IT neurons stay within the cerebrum, but can project to both ipsilateral and contralateral cortical and striatal locations. These pyramidal cell types constitute a microcircuit motif that is found in most regions in the neocortex, supporting a range of behavioural functions[17–19]. Impairments in these distinct types of pyramidal cells have been linked to neuropsychiatric disorders[16,20].

It is unclear how PT and IT neurons respond to psilocybin. Classic psychedelics are agonists at serotonin receptors. In response to serotonin, some pyramidal cells elevate spiking activity through 5-HT$_{2A}$ receptors, whereas other pyramidal cells suppress firing through 5-HT$_{1A}$ receptors[21,22]. It was reported that, in mouse brain slices, serotonin-evoked firing occurs in pyramidal cells with commissural projections (IT neurons), but not those with corticopontine projections (PT neurons)[23,24]. Transcript expression in the mouse frontal cortex corroborates this view—although PT and IT neurons both express *Htr2a*[25], there is more *Htr2a* in IT neurons[26]. However, another study performed in anaesthetized rats showed that psychedelics can excite midbrain-projecting pyramidal cells, which would constitute PT neurons[27]. Thus, the current literature provides conflicting clues towards how the main pyramidal cell types should contribute to psychedelic drug action.

Here we measured the acute and long-term effect of psilocybin on PT and IT neurons in the mouse medial frontal cortex in vivo. We found that PT neurons were the pyramidal cell type selectively driven by psilocybin to increase synaptic calcium transients and elevate spiking activity in awake mice. Moreover, although psilocybin evokes structural plasticity in both PT and IT neurons, causal manipulations indicate that frontal cortical PT neurons are needed for psilocybin's effects in stress-related

[1]Meinig School of Biomedical Engineering, Cornell University, Ithaca, NY, USA. [2]Department of Psychiatry, Yale University School of Medicine, New Haven, CT, USA. [3]Interdepartmental Neuroscience Program, Yale University School of Medicine, New Haven, CT, USA. [4]Medical Scientist Training Program, Yale University School of Medicine, New Haven, CT, USA. [5]Graduate School of Medical Science and Engineering, KAIST, Daejeon, Republic of Korea. [6]Department of Psychiatry, Weill Cornell Medicine, New York, NY, USA. [7]These authors contributed equally: Ling-Xiao Shao, Clara Liao. ✉e-mail: alex.kwan@cornell.edu

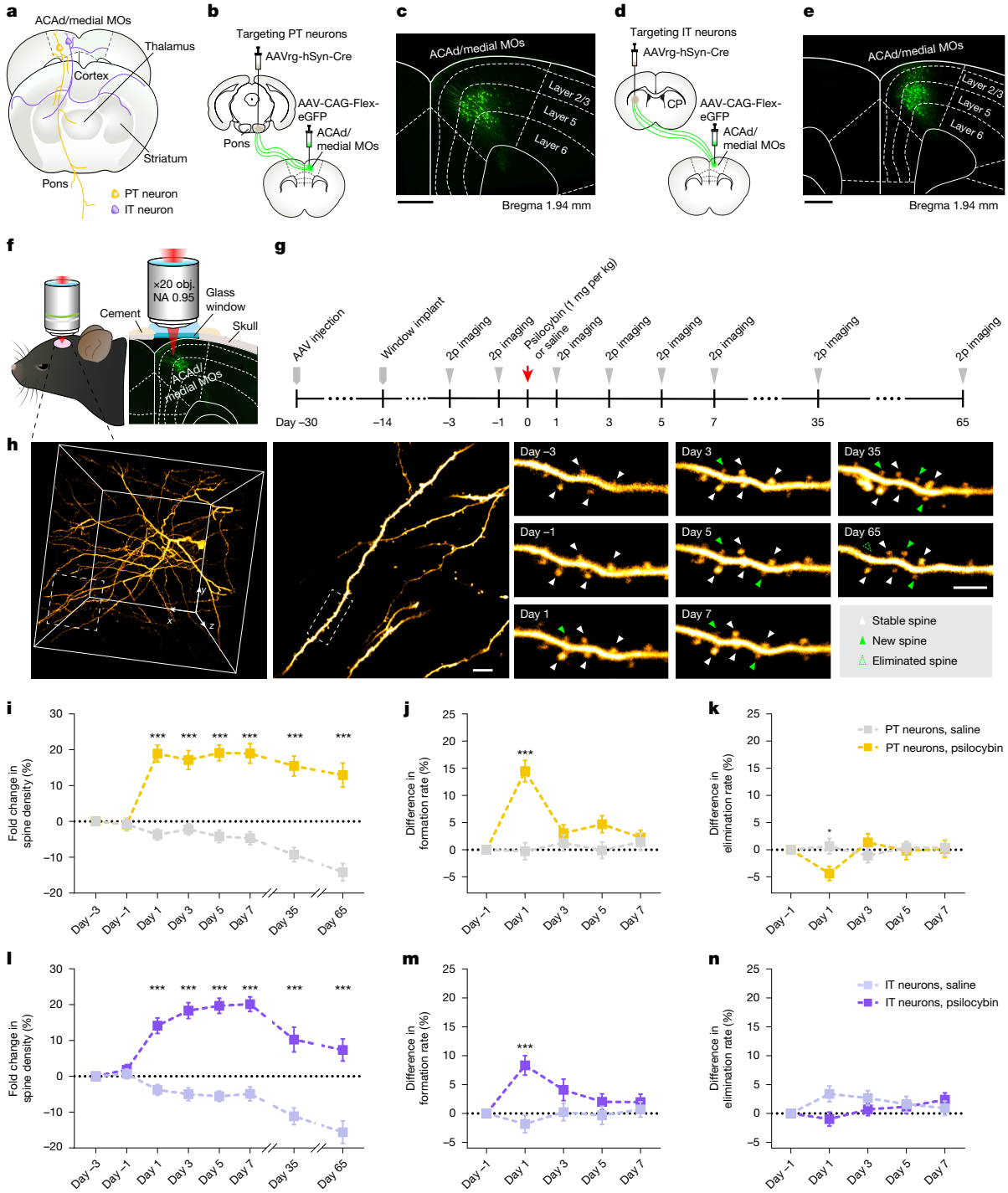

Fig. 1 | Psilocybin induces structural plasticity in both PT and IT types of frontal cortical pyramidal neurons. a, PT and IT neurons have different long-range projections. **b**,**c**, Schematic diagram (**b**) and image (**c**) of the strategy to express eGFP selectively in PT neurons in the medial frontal cortex. AAVrg, AAV serotype retrograde. **d**,**e**, Similar to **b** and **c**, respectively, but for IT neurons. CP, caudoputamen. **f**,**g**, Schematic (**f**) and timeline (**g**) of the longitudinal two-photon (2p) microscopy analysis. Obj., objective. **h**, Example field of view (FOV), tracking the same apical tuft dendrites for 65 days after treatment with psilocybin. **i**, The density of dendritic spines in the apical tuft of PT neurons after treatment with psilocybin (yellow; 1 mg per kg, i.p.) or saline (grey) across days, expressed as the fold change from the baseline in the first imaging session (day −3). **j**, The spine-formation rate was determined on the basis of the number of new and existing spines in consecutive imaging sessions across a two-day interval, expressed as the difference from the baseline in the first interval (day −3 to day −1). **k**, Similar to **j**, but for the elimination rate. For **i**–**k**, $n = 8$ (PT neurons, saline) and $n = 9$ (PT neurons, psilocybin) mice. **l**–**n**, The spine density (**l**), formation rate (**m**) and elimination rate (**n**), similar to **i**–**k**, respectively, but for IT neurons after treatment with psilocybin (purple) or saline (light purple). $n = 8$ mice per group. There was no cell type difference in psilocybin's effect on the spine density, formation rate or elimination rate. Data are mean ± s.e.m. across dendrites. For **i**–**n**, P values for the interaction effect of treatment × cell type indicated in the plots were calculated using a mixed-effects model: $P_{\text{treatment, cell type}} = 0.813$ (**i**,**l**), 0.580 (**j**,**m**) and 0.084 (**k**,**n**). Subsequently, post-hoc two-sample t-tests were used to compare the psilocybin and saline groups for each day. P values for post-hoc t-tests were adjusted using Bonferroni correction for multiple comparisons; $^*P < 0.05$, $^{***}P < 0.001$. Detailed sample size n values are provided in the Methods. Full statistics are provided in Supplementary Table 1. Scale bars, 500 µm (**d** and **e**), 10 µm (**h** (left)) and 5 µm (**h** (right)).

behavioural assays. Using conditional-knockout mice, we found that the 5-HT_{2A} receptor is required for psilocybin-evoked structural remodelling in PT neurons. The results therefore reveal that frontal cortical PT neurons and the 5-HT_{2A} receptor are essential components mediating psilocybin's long-term drug action in the brain.

Psilocybin-evoked structural plasticity

To sparsely express eGFP in PT or IT neurons for dendritic imaging, we injected a low titre of the retrogradely transported adeno-associated virus AAVretro-hSyn-Cre into the ipsilateral pons or contralateral striatum, and AAV-CAG-FLEX-eGFP into the medial frontal cortex of adult C57BL/6J mice (Fig. 1b,d and Extended Data Fig. 1). We focused on the cingulate and premotor portion of the medial frontal cortex, specifically the dorsal anterior cingulate area (ACAd) and the medial secondary motor area (medial MOs), because brain-wide FOS mapping indicates that the region robustly responds to stress[28] and psilocybin[29]. Histological analysis confirmed that eGFP-expressing cell bodies of PT neurons were restricted to deep cortical layers, whereas somata of IT neurons were spread across layers 2/3 and 5 (Fig. 1c,e), in agreement with the laminar distribution of the cell types[14,16]. We used two-photon microscopy to image through a chronically implanted glass window while the animal was anaesthetized. We visualized the same apical tuft dendrites located at 20–120 µm below the pial surface over multiple sessions across >2 months (Fig. 1f–h). At the baseline, PT neurons had a lower spine density but a higher spine head width compared with IT neurons (Extended Data Fig. 1).

For each of the four cell type and treatment conditions, we tracked and analysed 1,040–1,147 spines from 69–85 dendrites in 8–9 mice of both sexes. For statistical tests, mixed-effects models were used, which included random-effects terms to account for the nested nature of the data where spines are imaged from the same dendrites or same mouse. Details of the sample sizes and statistical tests for all of the experiments are provided in Supplementary Table 1. One dose of psilocybin (1 mg per kg, intraperitoneal (i.p.)) increased the spine density in both pyramidal cell types (PT, 19 ± 2% (psilocybin), −4 ± 2% (saline) on day 1; IT, 14 ± 2% (psilocybin), −4 ± 1% (saline); main effect of treatment, $P < 0.001$, mixed-effects model; Fig. 1i,l and Extended Data Fig. 2a–d,g,h). The elevated number of dendritic spines remained significant in the last imaging session at 65 days for psilocybin relative to the control. For both cell types, the higher spine density was driven by an increase in the rate of spine formation within 1 day after psilocybin (Fig. 1j,m and Extended Data Fig. 2e,i), with additionally a smaller decrease in spine elimination rate for PT neurons (Fig. 1k,n and Extended Data Fig. 2f,j).

The psilocybin-evoked structural remodelling occurred in mice of both sexes (Extended Data Fig. 2k–r). There was no change detected in spine protrusion length (Extended Data Fig. 2s–v). Owing to the sparse labelling, we could often trace the dendrites back to the cell body. Separately analysing IT neurons residing in layer 2/3 and layer 5 (Extended Data Fig. 3) indicated that the laminar position is not the reason for the difference observed across cell types. These results replicate our previous finding[7] that psilocybin increases the spine density in frontal cortical pyramidal cells, while extending the observation window to show that the change persists for >2 months in mice, which occurs for both the PT and IT subpopulations.

Essential role of frontal PT neurons

An important question is whether the frontal cortical cell types are relevant for psilocybin's behavioural effects. To answer this question, we expressed broadly and bilaterally inhibitory DREADD[30] in PT and IT neurons by injecting AAV-hSyn-DIO-hM4DGi-mCherry into adult *Fezf2-creER* and *Plxnd1-creER* mice (Fig. 2a,b). These tamoxifen-inducible Cre-driver lines target PT and IT neurons, respectively[31]. Control mice were injected with AAV-hSyn-DIO-mCherry. We treated the mice with the chemogenetic ligand deschloroclozapine[32] (DCZ; 0.1 mg per kg, i.p.) 15 min before injecting psilocybin (1 mg per kg, i.p.) or saline, thereby silencing the respective subsets of pyramidal cells when the drug is active in the brain.

We tested four behavioural assays. The head-twitch response is an indicator of hallucinogenic potency of a compound in humans[33] and occurs nearly immediately after the administration of psilocybin in rodents. Psilocybin induced head twitches in our mice as expected, and this was not affected by DREADD-mediated silencing of frontal cortical PT or IT neurons ($n = 11$–20 mice in each group; Fig. 2c–e and Extended Data Fig. 4). Next, learned helplessness is a preclinical paradigm that is relevant for modelling depression pathophysiology. Mice were exposed to inescapable foot shocks during two induction sessions and were subsequently tested for avoidance when faced with escapable foot shocks during a test session (Fig. 2f). A single dose of psilocybin reduced escape failures, suggesting that drug-treated animals were less affected by the uncontrollable stress (Fig. 2g,h). This psilocybin-induced relief of the stress-induced phenotype was abolished if frontal cortical PT neurons were silenced during drug administration (interaction effect of treatment and DREADD: $P < 0.001$, two-factor analysis of variance (ANOVA); $n = 13$–16 mice in each group; Fig. 2g and Extended Data Fig. 4). Meanwhile, inactivating IT neurons had no effect ($n = 11$–14 mice in each group; Fig. 2h and Extended Data Fig. 4). The tail-suspension test assesses stress-related escape, in which the immobility time serves as an indicator of stress-induced escape behaviour (Fig. 2i). Mice that were treated with psilocybin 24 h before testing showed a significant decrease in immobility time compared with the saline-treated mice, an improvement that was likewise abolished specifically by inactivation of frontal cortical PT neurons (interaction effect of treatment and DREADD: $P < 0.001$, two-factor ANOVA; $n = 9$–14 mice in each group; Fig. 2j,k and Extended Data Fig. 4). Finally, we found that frontal cortical PT neurons are needed for psilocybin-driven facilitation of fear extinction in chronically stressed mice (Extended Data Fig. 5). Together the behavioural data indicate that PT neurons in the medial frontal cortex are a key part of the brain's circuitry for mediating psilocybin's effect on stress-related behaviours.

Effects on dendritic Ca^{2+} signals

We next examined the early events that initiate the psilocybin-induced structural and behavioural adaptations. Calcium is a second messenger that regulates synaptic plasticity in pyramidal cells[34]. There are different plasticity mechanisms that depend on calcium elevations, both globally in dendritic branches[35] and locally in dendritic spines[36]. To determine whether calcium in dendritic branches and dendritic spines is involved in psilocybin's action, we used two-photon microscopy to image the apical dendrites of pyramidal cells in ACAd/medial MOs of awake, head-fixed mice. We focused on the acute phase of psilocybin action, imaging the same fields of view located at 20–120 µm below the pial surface for 10 min before and within 1 h after drug injection (Fig. 3a). To visualize calcium transients, we expressed the genetically encoded calcium indicator GCaMP6f in PT or IT neurons by injecting AAVretro-hSyn-Cre into the ipsilateral pons or contralateral striatum respectively, and AAV-CAG-FLEX-GCaMP6f into the medial frontal cortex (Fig. 3b,c). We used automated procedures[37] to detect calcium events in regions of interest corresponding to dendritic branches and dendritic spines before and after administering psilocybin (1 mg per kg, i.p.) or saline.

For dendritic branches, a single dose of psilocybin increased the rate of spontaneous calcium events in PT neurons (psilocybin, 23 ± 4%, $n = 149$ branches, 4 mice; saline, 5 ± 2%, $n = 140$ branches, 4 mice; Fig. 3d–f and Extended Data Figs. 6 and 7). Conversely, psilocybin did not affect calcium events in dendritic branches of IT neurons (psilocybin, −2 ± 3%, $n = 95$ branches, 3 mice; saline, 1 ± 3%, $n = 90$ branches, 3 mice; interaction effect of treatment × cell type, $P = 0.008$, mixed-effects model;

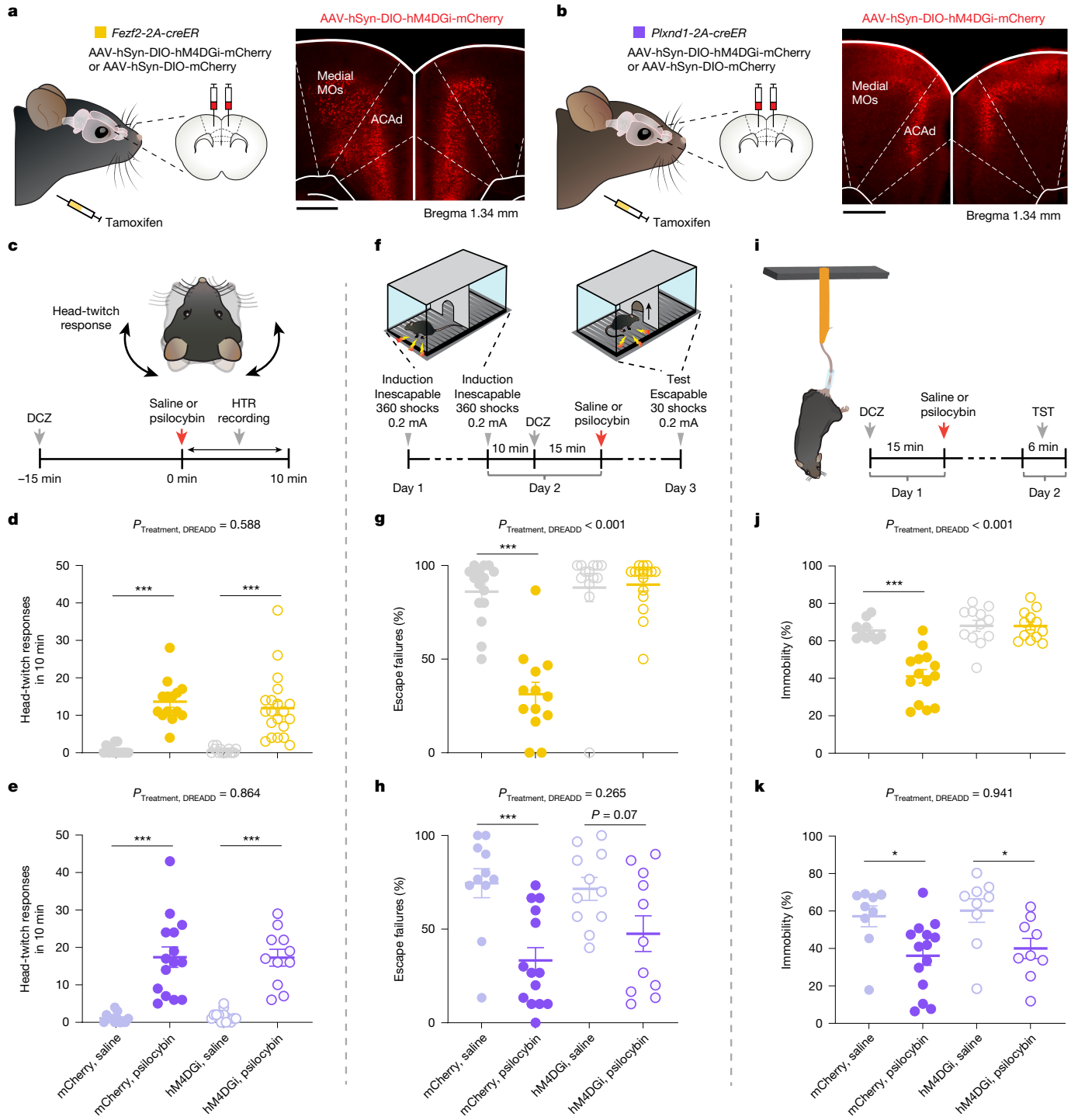

Fig. 2 | PT neurons are essential for psilocybin's effects on stress-related behaviours. a, Inhibitory chemogenetic receptor (hM4DGi) expressed in PT neurons in the medial frontal cortex of *Fezf2-creER* mice. **b**, Similar to **a**, but for IT neurons in *Plxnd1-creER* mice. **c**, Head-twitch response (HTR). **d**, The effect of PT neuron inactivation during psilocybin (1 mg per kg, i.p.) or saline administration. The circles represent individual animals. $n = 13$ (mCherry, saline), $n = 14$ (mCherry, psilocybin), $n = 15$ (hM4DGi, saline) and $n = 20$ (hM4DGi, psilocybin). **e**, Similar to **d**, but for IT neurons. $n = 12$ (mCherry, saline), $n = 15$ (mCherry, psilocybin), $n = 13$ (hM4DGi, saline) and $n = 11$ (hM4DGi, psilocybin). **f**, Learned helplessness. **g**, The effect of PT neuron inactivation during psilocybin or saline administration (interaction effect of treatment × DREADD: $P < 0.001$, two-factor ANOVA). The circles represent individual animals. $n = 15$ (mCherry, saline), $n = 13$ (mCherry, psilocybin), $n = 13$ (hM4DGi, saline) and $n = 16$ (hM4DGi, psilocybin). **h**, Similar to **g**, but for IT neurons. $n = 11$ (mCherry, saline), $n = 14$ (mCherry, psilocybin), $n = 11$ (hM4DGi, saline) and $n = 11$ (hM4DGi, psilocybin). **i**, Tail-suspension test (TST). **j**, The effect of PT neuron inactivation during psilocybin or saline administration on the subsequent proportion of time spent immobile (interaction effect of treatment × DREADD: $P < 0.001$, two-factor ANOVA). The circles represent individual mice. $n = 10$ (mCherry, saline), $n = 14$ (mCherry, psilocybin), $n = 12$ (hM4DGi, saline) and $n = 13$ (hM4DGi, psilocybin). **k**, Similar to **j**, but for IT neurons. $n = 9$ (mCherry, saline), $n = 14$ (mCherry, psilocybin), $n = 9$ (hM4DGi, saline) and $n = 9$ (hM4DGi, psilocybin). Data are mean ± s.e.m. across mice. For **d**,**e**,**g**,**h**,**j**,**k**, the P value for interaction effect of treatment and DREADD ($P_{\text{treatment, DREADD}}$) indicated above each plot was calculated using two-factor analysis of variance (ANOVA). Subsequently, post-hoc two-sample t-tests were used to compare the psilocybin and saline groups in mCherry mice and hM4DGi mice. P values from the post-hoc t-tests were adjusted using Bonferroni correction for multiple comparisons; $^*P < 0.05$, $^{***}P < 0.001$. Detailed sample size n values are provided in the Methods. Full statistics are provided in Supplementary Table 1. Scale bars, 500 µm (**a** and **b**).

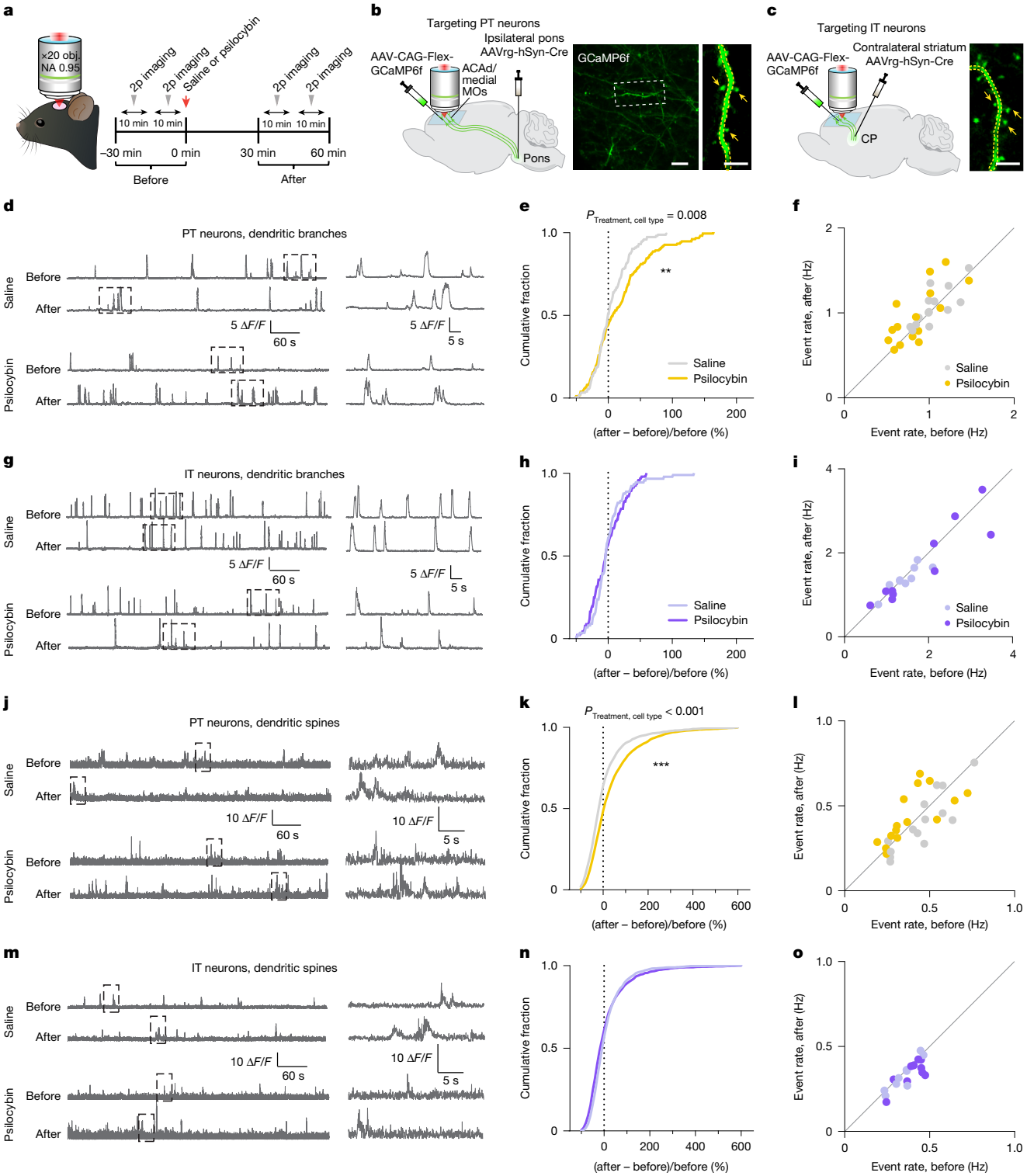

Fig. 3 | Psilocybin elevates the number of Ca^{2+} transients in dendritic branches and spines of PT neurons. a, Two-photon microscopy analysis of spontaneous dendritic calcium signals in awake mice. **b**, The viral strategy to express GCaMP6f selectively in PT neurons in the medial frontal cortex and an example in vivo image. **c**, Similar to **b**, but for IT neurons. **d**, $\Delta F/F_0$ from a PT dendritic branch before and after saline, and from a different branch before and after psilocybin (1 mg per kg, i.p.). Right, magnified views of the boxed areas on the left. **e**, Fractional change in the rate of calcium events detected in PT dendritic branches after psilocybin (yellow) or saline (grey). **f**, The raw rates of calcium events, averaged across dendritic branches in the same FOV, after psilocybin (yellow) or saline (grey). Each circle represents a FOV. **g**–**i**, Similar to **d**–**f**, respectively, but for IT dendritic branches. The colour keys in **e**, **f**, **h** and **i** also apply to **k**, **l**, **n** and **o**, respectively. **j**–**l**, Similar to **d**–**f**, respectively, but for PT dendritic spines. **m**–**o**, Similar to **d**–**f**, respectively, but for IT dendritic spines. For **f** and **l**, $n = 14$ FOVs from 4 mice (saline) and $n = 15$ FOVs from 4 mice (psilocybin). For **i** and **o**, $n = 9$ FOVs from 3 mice (saline) and $n = 10$ FOVs from 3 mice (psilocybin). For **e**,**h**,**k**,**n**, the P value for the interaction effect of treatment × cell type ($P_{\text{treatment, cell type}}$) indicated above each plot was calculated using a mixed-effects model. Subsequently, post-hoc two-sample t-tests were used to compare the psilocybin and saline groups in PT neurons and IT neurons. P values from the post-hoc t-tests were adjusted using Bonferroni correction for multiple comparisons; $^{**}P < 0.01$, $^{***}P < 0.001$. Detailed sample size n values are provided in the Methods. Full statistics are provided in Supplementary Table 1. Scale bars, 10 µm (**b** (left)) and 5 µm (**b** (right) and **c**).

Fig. 3g–i and Extended Data Figs. 6 and 7). For dendritic spines, we analysed fluorescence signals after subtracting the contribution from adjoining dendritic branch using a regression procedure[38,39] to estimate calcium transients arising from subthreshold synaptic activation. Similar to what we observed for dendritic branches, psilocybin elevated the rate of synaptic calcium events in dendritic spines of PT neurons (psilocybin, 68 ± 5%, n = 2,637 spines, 4 mice; saline, 37 ± 6%, n = 2,307 spines, 4 mice; Fig. 3j–l and Extended Data Figs. 6 and 7), but not in IT neurons (psilocybin, 20 ± 3%, n = 2,198 spines, 3 mice; saline, 16 ± 2%, n = 2,237 spines, 3 mice; interaction effect of treatment × cell type, P < 0.001, mixed-effects model; Fig. 3m–o and Extended Data Figs. 6 and 7). These data show that psilocybin preferentially boosts dendritic and synaptic calcium signalling in PT neurons in the medial frontal cortex.

Effects on spiking dynamics

The heightened dendritic calcium signals are probably due to increased dendritic excitability, which can lead to higher spiking activity in PT neurons. Alternatively, it has been shown that some 5-HT$_{1A}$ receptors localize to the axon initial segment[40], creating a scenario in which dendrites can be excitable while firing remains unchanged or suppressed in PT neurons. To disambiguate these possibilities, we used cell-type-specific electrophysiology to record from PT and IT neurons in awake, head-fixed mice. To identify the cell type, we expressed channelrhodopsin (ChR2) in PT or IT neurons by injecting AAV-EF1a-double floxed-hChR2(H134R)-eYFP into the medial frontal cortex of adult *Fezf2-creER* or *Plxnd1-creER* mice (Fig. 4a,b). We targeted the medial frontal cortex with a high-density Neuropixels probe[41] (Fig. 4c) and isolated single units by spike sorting and quality metrics (Extended Data Fig. 8a,b). We recorded for 30 min, injected psilocybin (1 mg per kg, i.p.) or saline, and then recorded for another 60 min. At the end of each recording session, we performed opto-tagging by applying trains of brief laser pulses (473 nm, 20 ms) to identify ChR2-expressing cells. The opto-tagged PT and IT neurons were reliably driven by the photostimulation to spike with short latency (Fig. 4d–f and Extended Data Fig. 8c–g).

A fraction of the opto-tagged PT neurons in *Fezf2-creER* mice responded vigorously to psilocybin. Specifically, 20% of the PT neurons substantially increased spiking activity, whereas few cells exhibited decrease after psilocybin or change after saline (psilocybin, 14 cells with post-drug mean z > 2, 2 cells with z < −2, n = 70 tagged neurons, 5 mice; saline, 2 cells with z > 2 and 3 cells with z < −2, n = 104 tagged neurons, 6 mice; Fig. 4g). On average, comparing before drug firing versus after drug firing, PT neurons showed significantly higher spike rates after psilocybin (P < 0.001, paired t-test with Bonferroni correction; Fig. 4h). By contrast, there was no notable change in the firing activity of IT neurons in *Plxnd1-creER* mice after psilocybin administration (psilocybin, 2 cells with z > 2, 0 cells with z < −2, n = 57 tagged neurons, 5 mice; saline, 2 cells with z > 2 and 0 cells with z < −2, n = 38 tagged neurons, 5 mice; P = 1.0, paired t-test with Bonferroni correction; Fig. 4i,j). These results show that psilocybin produces cell-type-specific changes in neural dynamics in the medial frontal cortex, highlighted by a set of PT neurons that responded acutely to drug administration by firing vigorously.

5-HT$_{2A}$ receptor is needed for behavioural changes

Our results thus far indicate that frontal cortical PT neurons are a target for psilocybin. We next investigated whether the cell type acts through 5-HT$_{2A}$ receptors. Current literature provides conflicting data on whether the 5-HT$_{2A}$ receptor is needed[8,42] or is non-essential[43,44] for the long-term neural and behavioural effects of psychedelics. The discrepancy may stem in part from the use of constitutive knockout animals and antagonist drugs, which can have unwanted effects on neurodevelopment or other receptors. Here we therefore took a different approach, using a conditional-knockout mouse, *Htr2a*$^{f/f}$ (encoding 5-HT$_{2A}$ receptor), for region- and cell-type-targeted deletion of 5-HT$_{2A}$ receptors in adult animals[45]. We first investigated whether there are 5-HT$_{2A}$ receptors in frontal cortical excitatory cell types. Analysis of Allen Institute's single cell sequencing data[46] revealed abundant *Htr2a* transcripts in a proportion of frontal cortical PT and IT neurons (Fig. 5a). Next, we validated Cre-mediated knockout of 5-HT$_{2A}$ receptors in *Htr2a*$^{f/f}$ mice. After injection of AAV-CaMKII-GFP-Cre into the medial frontal cortex, at the transcript level, analysis using quantitative PCR (qPCR) confirmed the absence of *Htr2a* transcripts in GFP$^+$ cells (control, 2 mice; knockout, 3 mice; Fig. 5b,c). At the synaptic level, we performed whole-cell recordings from GFP$^+$ layer 5 pyramidal cells, which did not exhibit a 5-HT-evoked increase in spontaneous excitatory postsynaptic currents (sEPSCs; control, 22 cells from 4 mice; knockout, 23 cells from 4 mice; Fig. 5d and Extended Data Fig. 9a,b), a 5-HT$_{2A}$-receptor-dependent phenomenon[47].

Using the *Htr2a*$^{f/f}$ mice, we investigated whether the 5-HT$_{2A}$ receptor in frontal cortical neurons is needed for psilocybin's effects in the same set of behaviours tested for Fig. 2. We injected either AAV-hSyn-Cre-P2A-dTomato or AAV-hSyn-eGFP bilaterally and broadly into the medial frontal cortex of *Htr2a*$^{f/f}$ mice. The mice with the localized knockout of 5-HT$_{2A}$ receptors exhibited the same amount of psilocybin-evoked head-twitch response as the controls (n = 6–9 mice in each group; Fig. 5e). The lack of dependence on the 5-HT$_{2A}$ receptor for the psilocybin-evoked head-twitch response was specific to local manipulation in the medial frontal cortex, because *Camk2a*^{cre}*Htr2a*$^{f/f}$ mice with constitutive and more widespread receptor knockout had markedly fewer head-twitch responses than control mice had after psilocybin administration (Extended Data Fig. 9c–e). Notably, the region-specific 5-HT$_{2A}$ receptor knockout was sufficient to render psilocybin ineffective for ameliorating the stress-related phenotypes in the learned-helplessness (n = 8–13 mice in each group; Fig. 5f) and tail-suspension (n = 8–9 mice in each group; Fig. 5g) tests. Note the caveat that, although the results from the head-twitch response and tail-suspension tests were clearly interpretable, the response of control animals to psilocybin in learned helplessness did not reach statistical significance, probably due to the floor effect from the low baseline rate of escape failures in this *Htr2a*$^{f/f}$ strain. Collectively, the data show the importance of 5-HT$_{2A}$ receptors in the medial frontal cortex for psilocybin's ameliorative effects on stress-related behaviour.

5-HT$_{2A}$R is needed for structural plasticity

We next investigated whether the 5-HT$_{2A}$ receptor is needed for psilocybin-evoked dendritic remodelling. To answer this question, we performed targeted knockout of 5-HT$_{2A}$ receptors by injecting low titre of AAVretro-hSyn-Cre into the ipsilateral pons and AAV-CAG-FLEX-eGFP into the medial frontal cortex of *Htr2a*$^{f/f}$ mice (Fig. 6a). In this viral strategy, the Cre recombinase was needed for dual purposes to express eGFP for visualization and to mediate knockout; the control animals therefore need the same viruses, which are injected into wild type C57BL/6J mice. We used two-photon microscopy to image the same apical tuft dendrites for four sessions, including before and after treatment with psilocybin (1 mg per kg, i.p.) or saline (Fig. 6b,c). For each condition (genotype and psilocybin or saline), we tracked and analysed 445–1,008 spines from 31–68 dendrites in 5–7 mice of both sexes. In agreement with our earlier findings, the frontal cortical PT neurons in control animals exhibited increased spine density after a single dose of psilocybin (spine density, 15 ± 2% (psilocybin), −2 ± 2% (saline), on day 1). By contrast, the cell-type-targeted 5-HT$_{2A}$ receptor knockout abolished psilocybin's effects (spine density: −1 ± 2% (psilocybin), 1 ± 2% (saline), on day 1; interaction effect of treatment × genotype: P = 0.01 for spine density, mixed-effects model; Fig. 6d–f and

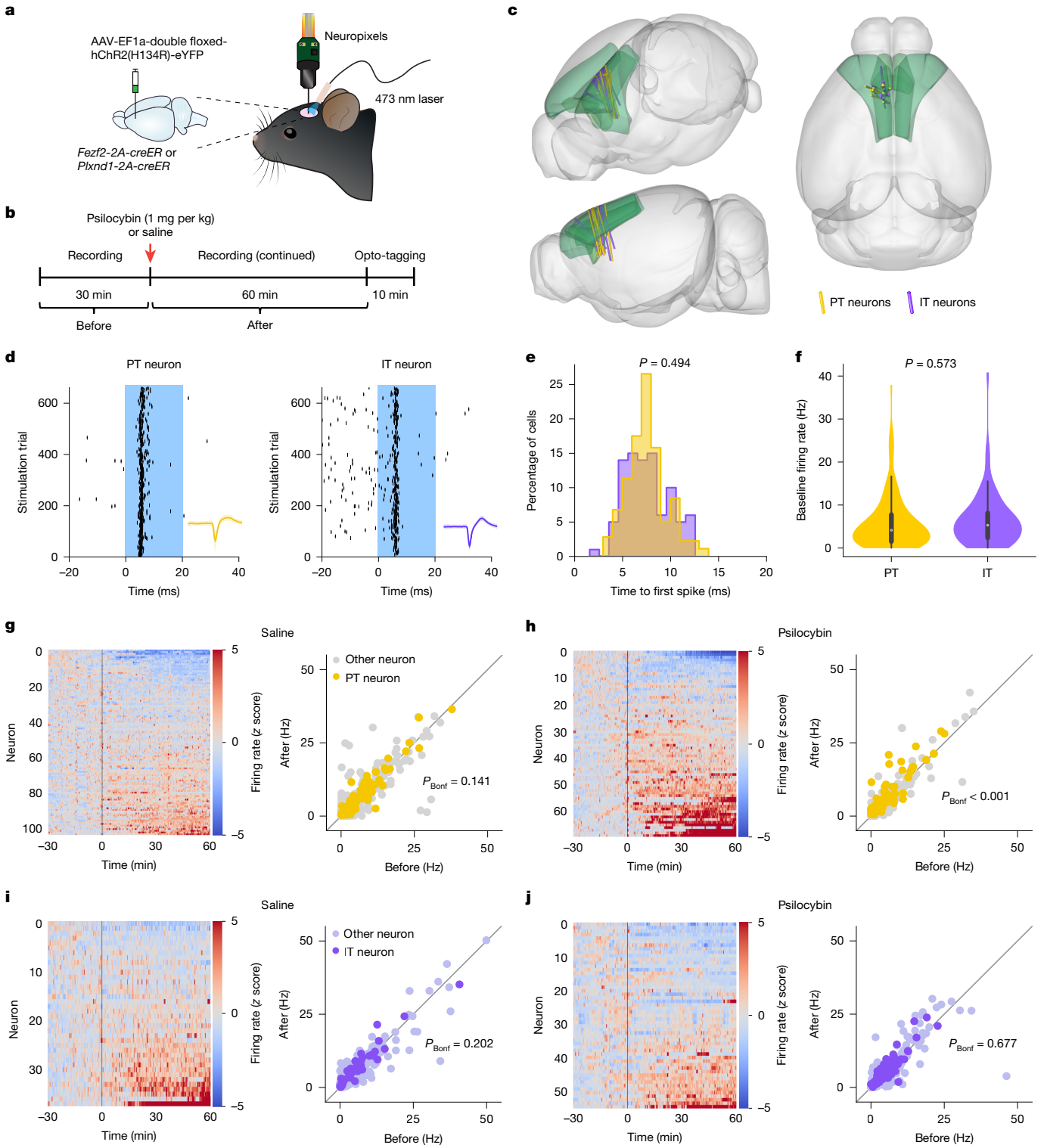

Fig. 4 | Psilocybin acutely increases firing in a subset of PT neurons in vivo. **a**, Neuropixel recording of ChR2-expressing neurons in *Fezf2-creER* and *Plxnd1-creER* mice. **b**, The experimental timeline, including the pre-drug (−30–0 min) and post-drug (0–60 min) periods. **c**, Probe tracks recovered from histological analysis and rendered in the Allen Mouse Brain Common Coordinate Framework. Green, ACAd and MOs. **d**, Spike raster of tagged neurons. Blue, laser stimulation. Inset: the mean waveform ± s.d. **e**, The time of the first spike relative to the onset of the laser for all tagged neurons. Yellow, *Fezf2-creER*; purple, *Plxnd1-creER*. **f**, The mean pre-drug firing rates of all of the tagged neurons. The patches show the symmetric kernel density estimate. The box plot within each patch indicates the median (centre line), the first and third quartiles (box limits), and the whiskers extend to the range within 1.5× the interquartile range. $n = 174$ tagged cells from 11 *Fezf2-creER* mice and $n = 95$ tagged cells from 10 *Plxnd1-creER* mice. **g**, The activity for all tagged neurons in *Fezf2-creER* mice before and after treatment with saline (left). The firing rate of each neuron was converted to a *z* score by normalization based on its pre-drug firing rate. Right, mean pre- and post-drug firing rates for all tagged (yellow) and untagged other neurons (grey) in *Fezf2-creER* mice treated with saline. Each dot represents one neuron. The colour keys in **g** and **i** also apply to **h** and **j**, respectively. **h**, Similar to **g**, but for psilocybin-treated *Fezf2-creER* mice. **i**,**j**, Similar to **g** and **h**, respectively, but for *Plxnd1-creER* mice. Statistical analysis: Kolmogorov–Smirnov test (**e**), unpaired *t*-test (**f**) and paired *t*-test (**g**–**j**). P_{Bonf}, Bonferroni-corrected *P* value. Detailed sample size *n* values are provided in the Methods. Full statistics are provided in Supplementary Table 1.

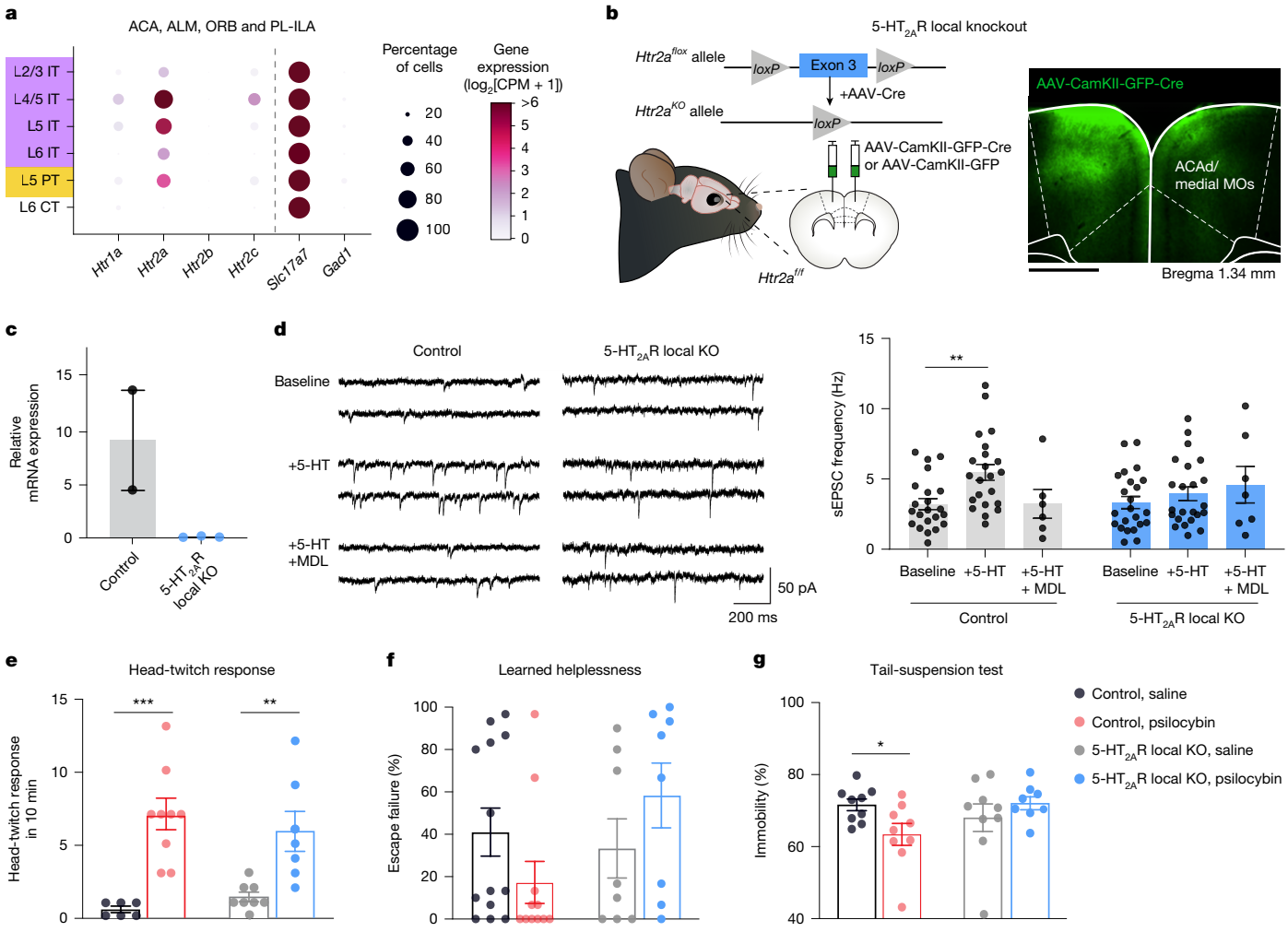

Fig. 5 | 5-HT$_{2A}$ receptors in the medial frontal cortex mediate psilocybin's alleviating effect on stress-related behaviours. a, Single-cell transcript counts summed from the mouse anterior cingulate area (ACA), anterior–lateral motor (ALM) region, orbital (ORB) region and prelimbic–infralimbic (PL-ILA) region, extracted from the SMART-Seq data from the Allen Institute. **b**, The viral injection strategy for inducing 5-HT$_{2A}$ receptor knockout or control in GFP$^+$ cells in the medial frontal cortex. Inset: post-hoc histological analysis. **c**, *Htr2a* mRNA levels in GFP$^+$ cells quantified using qPCR after fluorescence-activated cell sorting. The circles represent individual animals. $n = 2$ (control) and $n = 3$ (5-HT$_{2A}$R local KO). **d**, Whole-cell voltage-clamp recordings of spontaneous EPSCs from GFP$^+$ layer 5 pyramidal neurons at the baseline, after 20 µM 5-HT or after 5-HT and 100 nM MDL100907. The circles represent individual cells. Data are mean ± s.e.m. across cells. $n = 22$ (baseline), $n = 22$ (5-HT) and $n = 6$ (5-HT + MDL) cells from 4 mice in the control condition; and $n = 23$ (baseline), $n = 23$ (5-HT), $n = 7$ (5-HT + MDL) cells from 4 mice in the 5-HT$_{2A}$R local KO condition. **e**, The head-twitch response was measured in control animals after treatment with saline (grey) or psilocybin (red) and in 5-HT$_{2A}$R local KO animals after treatment with saline (light grey) or psilocybin (blue). The circles represent individual animals. Data are mean ± s.e.m. across mice. $n = 6$ (control, saline), $n = 9$ (control, psilocybin), $n = 8$ (5-HT$_{2A}$R local KO, saline) and $n = 7$ (5-HT$_{2A}$R local KO, psilocybin). **f**, Similar to **e**, but for learned helplessness. $n = 13$ (control, saline), $n = 11$ (control, psilocybin), $n = 8$ (5-HT$_{2A}$R local KO, saline) and $n = 8$ (5-HT$_{2A}$R local KO, psilocybin). **g**, Similar to **e**, but for tail suspension. $n = 9$ (control, saline), $n = 9$ (control, psilocybin), $n = 9$ (5-HT$_{2A}$R local KO, saline) and $n = 8$ (5-HT$_{2A}$R local KO, psilocybin). $^*P < 0.05$, $^{**}P < 0.01$, $^{***}P < 0.001$ (two-sided unpaired *t*-test; **d**–**g**). Full statistics are provided in Supplementary Table 1. Scale bar, 1 mm (**b**).

Extended Data Fig. 10). In vivo two-photon microscopy has a spatial resolution close to the limit needed for measuring spine size, motivating us to perform post-hoc confocal microscopy in fixed tissues from the same animals to determine psilocybin's impact on spine morphology ($n = 68$–136 dendrites from 3–7 mice in each group; Fig. 6g,h). Extracted from day 3 after psilocybin dosing, the confocal data showed a psilocybin-evoked increase in spine head width in apical tufts of frontal cortical PT neurons (0.53 ± 0.01 µm (psilocybin), 0.50 ± 0.01 µm (saline)), an effect that was absent when 5-HT$_{2A}$ receptors were selectively deleted (0.50 ± 0.01 µm (psilocybin), 0.51 ± 0.01 µm (saline); interaction effect of treatment × genotype: $P = 0.025$, two-factor ANOVA; Extended Data Fig. 10j). These data strongly point to the necessity of 5-HT$_{2A}$ receptors for psilocybin-induced structural neural plasticity.

Discussion

Here we demonstrate that psilocybin's long-term behavioural effects are dissociated at the level of pyramidal cell types in the frontal cortex. The cell-type-specific dissociation may be a mechanism leveraged by new psychedelic analogues to isolate therapeutic effects from hallucinogenic action[12,48,49]. A key finding is that frontal cortical PT neurons are essential for psilocybin's beneficial effects in stress-related phenotypes. The consequence for the structural plasticity in frontal cortical IT neurons is unclear; it may be an epiphenomenon, or the IT cell type may mediate other psilocybin-induced behavioural changes that were not tested in this study.

Our results emphasize the importance of 5-HT$_{2A}$ receptors for psilocybin's long-term effects. However, given that many PT and IT neurons

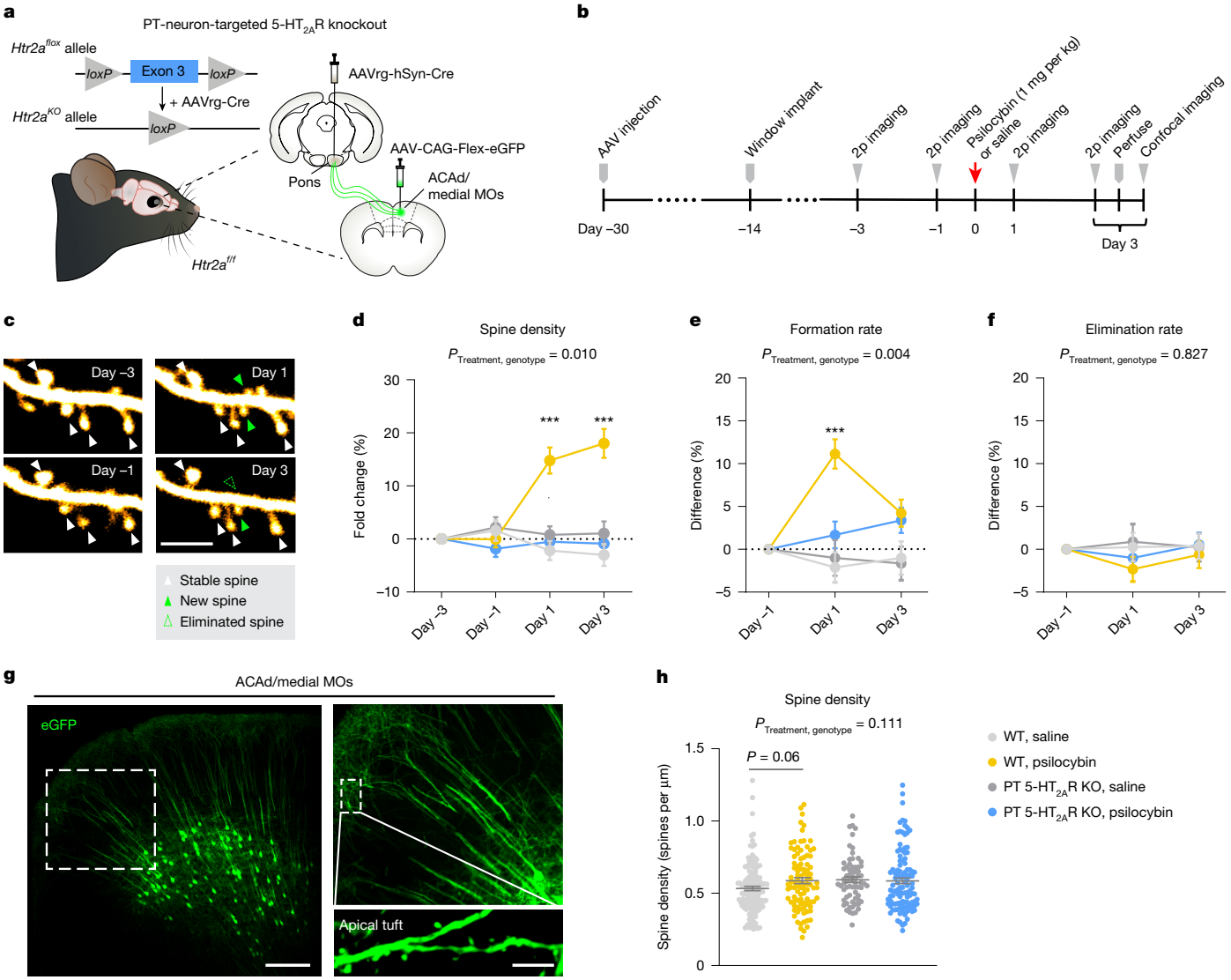

Fig. 6 | The 5-HT$_{2A}$ receptor is required for psilocybin-induced structural plasticity in PT neurons. a, The viral injection strategy for inducing conditional 5-HT$_{2A}$ receptor knockout and GFP expression for imaging in frontal cortical PT neurons. **b**, Longitudinal two-photon microscopy followed by confocal imaging. **c**, Example FOV tracking the same apical tuft dendrites before and after psilocybin treatment. **d**, The density of dendritic spines in the apical tuft of PT neurons across days, expressed as the fold change from the baseline in first imaging session (day −3) in wild-type mice after saline (light grey) or psilocybin (yellow) treatment and in mice with PT-neuron-targeted 5-HT$_{2A}$ receptor knockout after saline (grey) or psilocybin (blue) treatment. Post-hoc testing compared the WT + saline and WT + psilocybin groups per day; ***$P < 0.001$. **e**, The spine-formation rate was determined on the basis of the number of new and existing spines in consecutive imaging sessions across a two-day interval, expressed as difference from the baseline in first interval (day −3 to day −1; interaction effect of treatment × cell type: $P = 0.004$, mixed-effects model). Post-hoc testing compared the WT + saline and WT + psilocybin groups per day; ***$P < 0.001$. **f**, Similar to **e**, but for the elimination rate. For **d**–**f**, $n = 7$ (WT, saline), $n = 5$ (WT, psilocybin), $n = 5$ (PT 5-HT$_{2A}$R KO, saline) and $n = 6$ (PT 5-HT$_{2A}$R KO, psilocybin) mice. **g**, Example FOV imaging of apical tufts using confocal microscopy. **h**, The dendritic spine density in the apical tuft of PT neurons in wild-type mice after treatment with saline (light grey) or psilocybin (yellow) and in mice with PT neuron-targeted 5-HT$_{2A}$ receptor knockout after treatment with saline (grey) or psilocybin (blue). The circles represent individual dendritic segments. $n = 7$ (WT, saline), $n = 5$ (WT, psilocybin), $n = 3$ (PT 5-HT$_{2A}$R KO, saline) and $n = 5$ (PT 5-HT$_{2A}$R KO, psilocybin) mice. Statistical analysis was performed using two-factor ANOVA. *P* values from post-hoc tests were adjusted using Bonferroni correction for multiple comparisons; ***$P < 0.001$. Data are mean and s.e.m. across dendrites. Detailed sample size *n* values are provided in the Methods. Full statistics are provided in Supplementary Table 1. Scale bars 5 µm (**c** and **g** (right)) and 200 µm (**g** (left)).

in the frontal cortex have abundant *Htr2a* transcripts, the expression profile cannot fully explain why PT neurons respond preferentially to psilocybin. It is plausible that, under in vivo conditions, circuit mechanisms steer psilocybin's action to favour PT neurons. For example, psilocybin may heighten activity of certain long-range axonal inputs with biased connectivity to frontal cortical PT neurons, such as those from contralateral medial frontal cortex[50] and ventromedial thalamus[51]. Another possibility is that psilocybin may cause disinhibition by suppressing specific GABAergic neurons, such as deep-lying somatostatin-expressing interneurons that preferentially inhibit PT neurons[52,53]. Receptor and circuit mechanisms are not mutually exclusive and their relative contributions to psilocybin's impact on frontal cortical neural dynamics should be determined in future studies.

A hallmark of psychedelics is their ability to alter conscious perception. Layer 5 pyramidal cells, including specifically the PT neuron subpopulation, have been implicated in the transition from anaesthesia to wakefulness[54,55]. In the medial frontal cortex, PT neurons represent the subcortical output pathway, sending axons to ipsilateral thalamus and other deep-lying brain regions. There is growing interest to develop new treatments for depression that pair antidepressants with other

approaches, such as electroconvulsive or transcranial magnetic stimulation[56], with the goal of augmenting neural plasticity and enhancing the therapeutic outcome. This study delineates the cell types and receptors that underpin psychedelic action, highlighting the neural circuits that may be promising targets for neuromodulation and precision treatment.

Online content

Any methods, additional references, Nature Portfolio reporting summaries, source data, extended data, supplementary information, acknowledgements, peer review information; details of author contributions and competing interests; and statements of data and code availability are available at https://doi.org/10.1038/s41586-025-08813-6.

1. Goodwin, G. M. et al. Single-dose psilocybin for a treatment-resistant episode of major depression. *N. Engl. J. Med.* **387**, 1637–1648 (2022).
2. Davis, A. K. et al. Effects of psilocybin-assisted therapy on major depressive disorder: a randomized clinical trial. *JAMA Psychiatry* **78**, 481–489 (2021).
3. Carhart-Harris, R. et al. Trial of psilocybin versus escitalopram for depression. *N. Engl. J. Med.* **384**, 1402–1411 (2021).
4. Bogenschutz, M. P. et al. Percentage of heavy drinking days following psilocybin-assisted psychotherapy vs placebo in the treatment of adult patients with alcohol use disorder: a randomized clinical trial. *JAMA Psychiatry* **79**, 953–962 (2022).
5. Ly, C. et al. Psychedelics promote structural and functional neural plasticity. *Cell Rep.* **23**, 3170–3182 (2018).
6. Jones, K. A. et al. Rapid modulation of spine morphology by the 5-HT2A serotonin receptor through kalirin-7 signaling. *Proc. Natl Acad. Sci. USA* **106**, 19575–19580 (2009).
7. Shao, L. X. et al. Psilocybin induces rapid and persistent growth of dendritic spines in frontal cortex in vivo. *Neuron* **109**, 2535–2544 (2021).
8. de la Fuente Revenga, M. et al. Prolonged epigenomic and synaptic plasticity alterations following single exposure to a psychedelic in mice. *Cell Rep.* **37**, 109836 (2021).
9. Jefferson, S. J. et al. 5-MeO-DMT modifies innate behaviors and promotes structural neural plasticity in mice. *Neuropsychopharmacology* **48**, 1257–1266 (2023).
10. Kwan, A. C., Olson, D. E., Preller, K. H. & Roth, B. L. The neural basis of psychedelic action. *Nat. Neurosci.* **25**, 1407–1419 (2022).
11. Duman, R. S. & Aghajanian, G. K. Synaptic dysfunction in depression: potential therapeutic targets. *Science* **338**, 68–72 (2012).
12. Cameron, L. P. et al. A non-hallucinogenic psychedelic analogue with therapeutic potential. *Nature* **589**, 474–479 (2021).
13. Lu, J. et al. An analog of psychedelics restores functional neural circuits disrupted by unpredictable stress. *Mol. Psychiatry* **26**, 6237–6252 (2021).
14. Anastasiades, P. G. & Carter, A. G. Circuit organization of the rodent medial prefrontal cortex. *Trends Neurosci.* **44**, 550–563 (2021).
15. Baker, A. et al. Specialized subpopulations of deep-layer pyramidal neurons in the neocortex: bridging cellular properties to functional consequences. *J. Neurosci.* **38**, 5441–5455 (2018).
16. Shepherd, G. M. Corticostriatal connectivity and its role in disease. *Nat. Rev. Neurosci.* **14**, 278–291 (2013).
17. Li, N., Chen, T. W., Guo, Z. V., Gerfen, C. R. & Svoboda, K. A motor cortex circuit for motor planning and movement. *Nature* **519**, 51–56 (2015).
18. Musall, S. et al. Pyramidal cell types drive functionally distinct cortical activity patterns during decision-making. *Nat. Neurosci.* **26**, 495–505 (2023).
19. Tang, L. & Higley, M. J. Layer 5 circuits in V1 differentially control visuomotor behavior. *Neuron* **105**, 346–354 (2020).
20. Garcia, A. F., Crummy, E. A., Webb, I. G., Nooney, M. N. & Ferguson, S. M. Distinct populations of cortical pyramidal neurons mediate drug reward and aversion. *Nat. Commun.* **12**, 182 (2021).
21. Davies, M. F., Deisz, R. A., Prince, D. A. & Peroutka, S. J. Two distinct effects of 5-hydroxytryptamine on single cortical neurons. *Brain Res.* **423**, 347–352 (1987).
22. Araneda, R. & Andrade, R. 5-Hydroxytryptamine$_2$ and 5-hydroxytryptamine$_{1A}$ receptors mediate opposing responses on membrane excitability in rat association cortex. *Neuroscience* **40**, 199–412 (1991).
23. Avesar, D. & Gulledge, A. T. Selective serotonergic excitation of callosal projection neurons. *Front. Neural Circuits* **6**, 12 (2012).
24. Elliott, M. C., Tanaka, P. M., Schwark, R. W. & Andrade, R. Serotonin differentially regulates L5 pyramidal cell classes of the medial prefrontal cortex in rats and mice. *eNeuro* https://doi.org/10.1523/ENEURO.0305-17.2018 (2018).
25. Amargos-Bosch, M. et al. Co-expression and *in vivo* interaction of serotonin$_{1A}$ and serotonin$_{2A}$ receptors in pyramidal neurons of prefrontal cortex. *Cereb. Cortex* **14**, 281–299 (2004).
26. Savalia, N. K., Shao, L. X. & Kwan, A. C. A dendrite-focused framework for understanding the actions of ketamine and psychedelics. *Trends Neurosci.* **44**, 260–275 (2021).
27. Puig, M. V., Celada, P., Diaz-Mataix, L. & Artigas, F. *In vivo* modulation of the activity of pyramidal neurons in the rat medial prefrontal cortex by 5-HT$_{2A}$ receptors: relationship to thalamocortical afferents. *Cereb. Cortex* **13**, 870–882 (2003).
28. Kim, Y. et al. Whole-brain mapping of neuronal activity in the learned helplessness model of depression. *Front. Neural Circuits* **10**, 3 (2016).
29. Davoudian, P. A., Shao, L. X. & Kwan, A. C. Shared and distinct brain regions targeted for immediate early gene expression by ketamine and psilocybin. *ACS Chem. Neurosci.* **14**, 468–480 (2023).
30. Armbruster, B. N., Li, X., Pausch, M. H., Herlitze, S. & Roth, B. L. Evolving the lock to fit the key to create a family of G protein-coupled receptors potently activated by an inert ligand. *Proc. Natl Acad. Sci. USA* **104**, 5163–5168 (2007).
31. Matho, K. S. et al. Genetic dissection of the glutamatergic neuron system in cerebral cortex. *Nature* **598**, 182–187 (2021).
32. Nagai, Y. et al. Deschloroclozapine, a potent and selective chemogenetic actuator enables rapid neuronal and behavioral modulations in mice and monkeys. *Nat. Neurosci.* **23**, 1157–1167 (2020).
33. Halberstadt, A. L., Chatha, M., Klein, A. K., Wallach, J. & Brandt, S. D. Correlation between the potency of hallucinogens in the mouse head-twitch response assay and their behavioral and subjective effects in other species. *Neuropharmacology* **167**, 107933 (2020).
34. Malenka, R. C., Lancaster, B. & Zucker, R. S. Temporal limits on the rise in postsynaptic calcium required for the induction of long-term potentiation. *Neuron* **9**, 121–128 (1992).
35. Bittner, K. C., Milstein, A. D., Grienberger, C., Romani, S. & Magee, J. C. Behavioral time scale synaptic plasticity underlies CA1 place fields. *Science* **357**, 1033–1036 (2017).
36. Lee, S. J., Escobedo-Lozoya, Y., Szatmari, E. M. & Yasuda, R. Activation of CaMKII in single dendritic spines during long-term potentiation. *Nature* **458**, 299–304 (2009).
37. Friedrich, J., Zhou, P. & Paninski, L. Fast online deconvolution of calcium imaging data. *PLoS Comput. Biol.* **13**, e1005423 (2017).
38. Ali, F. et al. Ketamine disinhibits dendrites and enhances calcium signals in prefrontal dendritic spines. *Nat. Commun.* **11**, 72 (2020).
39. Chen, T. W. et al. Ultrasensitive fluorescent proteins for imaging neuronal activity. *Nature* **499**, 295–300 (2013).
40. DeFelipe, J., Arellano, J. I., Gomez, A., Azmitia, E. C. & Munoz, A. Pyramidal cell axons show a local specialization for GABA and 5-HT inputs in monkey and human cerebral cortex. *J. Comp. Neurol.* **433**, 148–155 (2001).
41. Jun, J. J. et al. Fully integrated silicon probes for high-density recording of neural activity. *Nature* **551**, 232–236 (2017).
42. Cameron, L. P. et al. 5-HT2ARs mediate therapeutic behavioral effects of psychedelic tryptamines. *ACS Chem. Neurosci.* **14**, 351–358 (2023).
43. Hesselgrave, N., Troppoli, T. A., Wulff, A. B., Cole, A. B. & Thompson, S. M. Harnessing psilocybin: antidepressant-like behavioral and synaptic actions of psilocybin are independent of 5-HT2R activation in mice. *Proc. Natl Acad. Sci. USA* **118**, e2022489118 (2021).
44. Sekssaoui, M., Bockaert, J., Marin, P. & Bécamel, C. Antidepressant-like effects of psychedelics in a chronic despair mouse model: is the 5-HT$_{2A}$ receptor the unique player? *Neuropsychopharmacology* **49**, 747–756 (2024).
45. Choi, W. et al. Serotonin signals through a gut-liver axis to regulate hepatic steatosis. *Nat. Commun.* **9**, 4824 (2018).
46. Yao, Z. et al. A taxonomy of transcriptomic cell types across the isocortex and hippocampal formation. *Cell* **184**, 3222–3241 (2021).
47. Aghajanian, G. K. & Marek, G. J. Serotonin induces excitatory postsynaptic potentials in apical dendrites of neocortical pyramidal cells. *Neuropharmacology* **36**, 589–599 (1997).
48. Kaplan, A. L. et al. Bespoke library docking for 5-HT$_{2A}$ receptor agonists with antidepressant activity. *Nature* **610**, 582–591 (2022).
49. Cao, D. et al. Structure-based discovery of nonhallucinogenic psychedelic analogs. *Science* **375**, 403–411 (2022).
50. Dembrow, N. C., Zemelman, B. V. & Johnston, D. Temporal dynamics of L5 dendrites in medial prefrontal cortex regulate integration versus coincidence detection of afferent inputs. *J. Neurosci.* **35**, 4501–4514 (2015).
51. Anastasiades, P. G., Collins, D. P. & Carter, A. G. Mediodorsal and ventromedial thalamus engage distinct L1 circuits in the prefrontal cortex. *Neuron* **109**, 314–330 (2021).
52. Silberberg, G. & Markram, H. Disynaptic inhibition between neocortical pyramidal cells mediated by Martinotti cells. *Neuron* **53**, 735–746 (2007).
53. Wu, S. J. et al. Cortical somatostatin interneuron subtypes form cell-type-specific circuits. *Neuron* **111**, 2675–2692 (2023).
54. Suzuki, M. & Larkum, M. E. General anesthesia decouples cortical pyramidal neurons. *Cell* **180**, 666–676 (2020).
55. Bharioke, A. et al. General anesthesia globally synchronizes activity selectively in layer 5 cortical pyramidal neurons. *Neuron* **110**, 2024–2040 (2022).
56. Wilkinson, S. T., Holtzheimer, P. E., Gao, S., Kirwin, D. S. & Price, R. B. Leveraging neuroplasticity to enhance adaptive learning: the potential for synergistic somatic-behavioral treatment combinations to improve clinical outcomes in depression. *Biol. Psychiatry* **85**, 454–465 (2019).

Methods

Animals

Wild-type C57BL/6J (000664), *Fezf2-2A-creER*[31] (*B6;129S4-Fezf2*$^{tm1.1(cre/ERT2)Zjh}$*/J*, 036296), *Plxnd1-2A-creER*[31] (*B6;129S4-Plxnd1*$^{tm1.1(cre/ERT2)Zjh/J}$, 036296), *Thy1*^{GFP} line M[57] (*Tg(Thy1-eGFP)MJrs/J*, 007788), and *Camk2a*^{cre} (*B6.Cg-Tg(Camk2a-cre)T29-1Stl/J*, 005359) mice were from Jackson Laboratory and bred in our animal facility. *Htr2a*$^{f/f}$ mice were described in a previous study[45] and bred in our animal facility. For behavioural and electrophysiological studies involving PT and IT neurons, homozygous *Fezf2-2A-creER* and *Plxnd1-2A-creER* mice (5–8 weeks) were used for viral injection, then tested 2 weeks later. For two-photon imaging studies, C57BL/6J or homozygous *Htr2a*$^{f/f}$ mice (aged 5–7 weeks) were used for viral injection, then implanted with a glass window and imaged 2–3 weeks later. For validation and behavioural studies involving the *Htr2a*$^{f/f}$ mice, homozygous *Htr2a*$^{f/f}$ mice or littermate controls (aged 5–8 weeks) were used for viral injection, then tested 3 weeks later. Mice were housed in groups with 2–5 mice per cage in a temperature-controlled room, operating under a normal 12 h–12 h light–dark cycle (08:00 to 20:00 for light), at 70–72 °F ambient temperature and 30–70% humidity. Food and water were available ad libitum. Animals were randomly assigned to different experimental groups. Animal care and experimental procedures were approved by the Institutional Animal Care & Use Committee (IACUC) at Cornell University and Yale University.

Viruses

AAV1-pCAG-FLEX-eGFP-WPRE (51502), AAVretro-hSyn-Cre-WPRE-hGH (105553), AAV1-CAG-Flex-GCaMP6f-WPRE-SV40 (100835), AAV1-hSyn-DIO-hM4D(Gi)-mCherry (44362), AAV1-hSyn-DIO-mCherry (50459), AAV1-EF1a-double floxed-hChR2(H134R)-eYFP-WPRE-HGHpA (20298), AAV9-CaMKII-HI-GFP-Cre.WPRE.SV40 (105551), AAV8-CaMKIIa-eGFP (50469), AAV9-hSyn-Cre-P2A-dTomato (107738) and AAV9-hSyn-eGFP (50465) were purchased from Addgene. AAVretro is an AAV designed for efficient retrograde transport[58]. All viruses had titres of $\geq 7 \times 10^{12}$ viral genomes per ml. The viruses were stored at −80 °C. Before stereotaxic injection, they were taken out of the −80 °C freezer, thawed on ice and diluted to the corresponding titre for injection.

Surgery

Before surgery, each mouse was injected with dexamethasone (3 mg per kg, intramuscular; DexaJect, 002459, Henry Schein Animal Health) and carprofen (5 mg per kg, subcutaneous; 024751, Henry Schein Animal Health) for anti-inflammatory and analgesic purposes. At the start of surgery, anaesthesia was induced with 2–3% isoflurane and the mouse was affixed in a stereotaxic apparatus (Model 900, David Kopf Instruments). Anaesthesia was maintained with 1–1.5% isoflurane. Body temperature was maintained at 38 °C using a far-infrared warming pad (RT-0515, Kent Scientific). Petrolatum ophthalmic ointment (IS4398, Dechra) was applied to cover the eyes. The hair on the head was shaved. The scalp was disinfected by wiping with ethanol pads and povidone-iodine. Small burr holes were made above the targeted brain regions using a handheld dental drill (HP4-917, Foredom). AAV was delivered intracranially into the brain by inserting a borosilicate glass capillary and using an injector (Nanoject II Auto-Nanoliter Injector, Drummond Scientific). Injections were done for the various experiments using different viruses and volumes, as specified in the paragraphs below, using 4.6 nl pulses with a 20 s interval between each pulse. To reduce the backflow of the virus, we waited 5–10 min after completing an injection at one site before retracting the pipette to move on to the next site. For the medial frontal cortex and striatum, the stereotaxic apparatus was positioned at four sites corresponding to four vertices of a 0.2-mm-wide square centred at the coordinates mentioned below. Throughout the procedure, the brain surface was kept moist with artificial cerebrospinal fluid (aCSF; 135 mM NaCl, 5 mM HEPES, 5 mM KCl, 1.8 mM $CaCl_2$, 1 mM $MgCl_2$; pH 7.3). After injections, the craniotomies were covered with silicone elastomer (0318, Smooth-On), and the skin was sutured (1265B, Surgical Specialties). At the end of surgery, the animal was given carprofen (5 mg per kg, subcutaneous) immediately and then again once on each of the following 3 days.

For two-photon imaging of the dendritic structure, to target PT neurons, 110.4 nl of AAVretro-hSyn-Cre-WPRE-hGH (1:100 diluted in PBS (P4417, Sigma-Aldrich)) was injected into the pons (anteroposterior (AP), −3.4 mm; mediolateral (ML), −0.7 mm; dorsoventral (DV), −5.2 mm; relative to bregma; the same applies below, unless otherwise specified) and 92 nl of AAV1-pCAG-FLEX-eGFP-WPRE (1:20 diluted in PBS) was injected into the ACAd and medial MOs subregion of medial frontal cortex (AP, 1.5 mm; ML, −0.4 mm; DV, −1.0 mm) of a C57BL/6J or a *Htr2a*$^{f/f}$ mouse. To target IT neurons, 101.2 nl of AAVretro-hSyn-Cre-WPRE-hGH (1:100 diluted in PBS) was injected into the contralateral striatum (AP, 0.6 mm; ML, 2.2 mm; DV, −2.8 mm) and 92 nl of AAV1-pCAG-FLEX-eGFP-WPRE (1:20 diluted in PBS) was injected into the medial frontal cortex of a C57BL/6J mouse. After 2–3 weeks, the mouse underwent a second procedure, with the same pre- and post-operative care, to implant a glass window for imaging. An incision was made to remove skin above the skull, and the skull was cleaned to remove connective tissues. A dental drill was used to make an approximately 3-mm-diameter circular craniotomy above the previously targeted location at the medial frontal cortex. aCSF was used to immerse the exposed dura in the craniotomy. A two-layer glass window was made by bonding two round coverslips (3 mm diameter, 0.15 mm thickness; 640720, Warner Instruments) with ultraviolet light-curing optical adhesive (NOA 61, Norland Products) using an ultraviolet illuminator (2182210, Loctite). The glass window was placed over the craniotomy and, while maintaining a slight pressure, super glue adhesive (Henkel Loctite 454) was carefully used to secure the window to the surrounding skull. A stainless steel headplate (eMachineShop; design available at https://github.com/Kwan-Lab/behavioural-rigs) was secured onto the skull and centred on the glass window using a quick adhesive cement system (Metabond, Parkell). The mouse would recover for at least 10 days after the window implant prior to imaging experiments.

For two-photon imaging of dendritic calcium transients, to target PT neurons, 110.4 nl of AAVretro-hSyn-Cre-WPRE-hGH (1:10 diluted in PBS) was injected into the pons, and 92 nl of AAV1-CAG-Flex-GCaMP6f-WPRE-SV40 (1:10 diluted in PBS) was injected into medial frontal cortex of a C57BL/6J mouse. To target IT neurons, 110.4 nl of AAVretro-hSyn-Cre-WPRE-hGH (1:10 diluted in PBS) was injected into contralateral striatum and 92 nl of AAV1-CAG-Flex-GCaMP6f-WPRE-SV40 (1:10 diluted in PBS) was injected into medial frontal cortex of a C57BL/6J mouse. For two-photon imaging of dendritic structure in *Thy1*^{GFP} mice, 345 nl of AAV9-hSyn-Cre-P2A-dTomato (1:100 diluted in PBS) was injected into the medial frontal cortex of *Thy1*^{GFP}*Htr2a*$^{f/f}$ or *Thy1*^{GFP}*Htr2a*$^{WT/WT}$ mice. The surgical procedures were the same as above.

For chemogenetic experiments, 276 nl of AAV1-hSyn-DIO-hM4D(Gi)-mCherry or the control virus AAV1-hSyn-DIO-mCherry was injected into the medial frontal cortex bilaterally (AP, 1.5 mm; ML, 0.4 and −0.4 mm; DV, −1.0 and −1.2 mm) of *Fezf2-2A-creER* mice to target PT neurons and *Plxnd1-2A-creER* mice to target IT neurons. For in vivo electrophysiology, 276 nl of AAV1-EF1a-double floxed-hChR2(H134R)-eYFP was injected into the medial frontal cortex unilaterally (AP, 1.5 mm; ML, 0.4 mm; DV, −1.0 and −1.2 mm) of *Fezf2-creER* and *Plxnd1-creER* mice to target PT and IT neurons, respectively. After 2 weeks, the mouse would undergo a second procedure. An incision was made to remove the skin and the periosteum was cleared. A dental drill was used to make a 0.9 mm craniotomy and a 0.86 mm self-tapping bone screw (19010-10, Fine Science Tools) was placed through the skull bone into the cerebellum to act as a ground screw and provide further structural support for head-fixation. A custom stainless steel headplate was affixed onto the skull using a quick adhesive cement system. The mouse would recover for at least 1 week after surgery before commencement

of electrophysiological experiments. In both cases, injection of AAVs were made before administration of tamoxifen.

For validation of the *Htr2a*$^{f/f}$ mouse line, homozygous *Htr2a*$^{f/f}$ animals were bilaterally injected with AAV9-CaMKII-HI-GFP-Cre.WPRE.SV40 (441.6 nl, 1:10 diluted in PBS) or AAV8-CaMKIIa-eGFP (441.6 nl, 1:10 diluted in PBS) in the medial frontal cortex (AP, 1.5 mm; ML, ±0.4 mm; DV, −0.4, −0.6 and −1.2 mm, relative to dura). Incised skin was sutured. Animals would recover for at least 3 weeks before euthanasia for transcript or slice electrophysiology experiments. For behavioural experiments involving *Htr2a*$^{f/f}$ mice, homozygous *Htr2a*$^{f/f}$ animals were bilaterally injected with AAV9-hSyn-Cre-P2A-dTomato (690 nl, 1:50 diluted in PBS) or AAV9-hSyn-eGFP (690 nl, 1:50 diluted in PBS) in the medial frontal cortex (AP, 1.5 mm; ML, −0.4 mm; DV, −0.4, −0.6 and −1.2 mm, relative to dura). Incised skin was sutured. Animals would recover for at least 3 weeks before behavioural experiments.

Tamoxifen

Tamoxifen was used for inducible Cre-dependent gene expression in *Fezf2-creER* and *Plxnd1-creER* mice. Tamoxifen (T5648, Sigma-Aldrich) was dissolved in corn oil (C8267, Sigma-Aldrich) at concentration of 20 mg ml^{-1} in an ultrasonic bath at 37 °C for 1–4 h. The solution was then aliquoted into 1 ml tubes, wrapped with aluminium foil and stored at −20 °C. For injections, the tamoxifen aliquots were thawed at 4 °C. Each animal was weighed and received tamoxifen (75 mg per kg, i.p.) once every 24 h for 5 consecutive days. Experiments involving inducible Cre expression were conducted at least 2 weeks after the last dose of tamoxifen to allow time for viral-mediated expression.

Histology

Histology was performed to determine the accuracy of injection locations and assess transgene expression. For two-photon imaging and behavioural studies, after completion of experiments, mice were perfused with PBS, followed by paraformaldehyde solution (PFA, 4% (v/v) in PBS). The brains were extracted and further fixed in 4% PFA at 4 °C for 12–24 h. Subsequently, 40-μm-thick coronal sections were obtained using a vibratome (VT1000S, Leica) and mounted onto slides with glass coverslips. The sections were imaged using a wide-field fluorescence microscope (BZ-X810, Keyence). For electrophysiology, the coronal sections were prepared similarly, mounted onto slides using Vectashield containing DAPI (H-1200-10, Vector Laboratories) and imaged. To locate the Neuropixels probe, we used SHARP-TRACK[59] to align the images of the coronal sections, including the DiI tracks, with the standardized Allen Common Coordinate Framework 6 (ref. 60). Reconstructed probe tracks were visualized within the Allen Common Coordinate Framework using Brainrender[61].

Two-photon imaging

Two-photon imaging experiments were performed using a Movable Objective Microscope (MOM, Sutter Instrument) equipped with a resonant-galvo scanner (Rapid Multi Region Scanner, Vidrio Technologies) and a water-immersion ×20 objective (XLUMPLFLN, ×20/0.95 NA, Olympus). ScanImage 2020 software[62] was used to control the microscope for image acquisition. To visualize GFP- or GCaMP6f-expressing dendrites, a tuneable Ti:Sapphire femtosecond laser (Chameleon Ultra II, Coherent) was used as the excitation source. The excitation wavelength was set at 920 nm, and emission was collected behind a 475- to 550-nm band-pass filter for fluorescence from GFP or GCaMP6f. The laser power measured at the objective was typically ≤40 mW and varied depending on the imaging depth. When imaging of the same FOV across days, the laser power was kept the same in each imaging session.

For structural imaging of dendrites, in each imaging session, the mouse was head fixed and anaesthetized with 1% isoflurane through a nose cone. The body temperature was maintained at 37.4 °C through a heating pad system (40-90-8D, FHC) with feedback control from a rectal thermistor probe. Each imaging session lasted 0.5–1.5 h. To target the ACAd and medial MOs subregion of the medial prefrontal cortex, we imaged within 400 μm of the midline as determined by first visualizing the sagittal sinus in bright-field imaging. To target apical tuft dendrites, we first imaged 0–200 μm below the pial surface to identify the apical tuft dendrites and apical trunk, and then select apical tuft dendrites located between 20–120 μm below the pial surface for longitudinal imaging. Multiple different fields of view were imaged in the same mouse. For each FOV, 10- to 40-μm-thick *z* stacks were collected with 1-μm steps using 15 Hz bidirectional scanning at 1,024 × 1,024 pixels with a resolution of 0.11 μm per pixel. Each mouse was imaged at the same fields of view on day −3, −1, 1, 3, 5, 7, 35 and 65 relative to the day of drug administration. On the day of treatment (day 0), no imaging was performed and the mouse was injected while awake with either psilocybin (1 mg per kg, i.p.; prepared from working solution, which was made fresh monthly from powder; Usona Institute) or saline (10 ml per kg, i.p.). After injection, the mouse was placed into a clean cage, and head twitches were visually inspected for 10 min before returning the mice to their home cage. At the end of the imaging session, for the purpose of reconstructing the apical dendritic trees, a *z* stack was acquired between 0 and 900 μm below the dura with 2 μm steps. For structural imaging of dendrites, 148 dendrites from 17 C57BL/6J mice were imaged for psilocybin (8 male, including 5 for PT and 3 for IT neurons; 9 female, including 4 for PT and 5 for IT neurons), and 154 dendrites from 16 C57BL/6J mice were imaged for saline (7 male, including 4 for PT and 3 for IT neurons; 9 female, including 4 for PT and 5 for IT neurons). For structural imaging to test the effects of 5-HT$_{2A}$ receptor knockout on dendrites, 117 dendrites from 11 mice were imaged for psilocybin (6 *Htr2a*$^{f/f}$ mice; 5 C57BL/6J mice), and 80 dendrites from 12 mice were imaged for saline (5 *Htr2a*$^{f/f}$ mice; 7 C57BL/6J mice). For structural imaging of *Thy1*^{GFP} mice, 38 dendrites from 2 *Thy1*^{GFP}*Htr2a*$^{WT/WT}$ mice were imaged for psilocybin, 49 dendrites from 5 *Thy1*^{GFP}*Htr2a*$^{f/f}$ mice were imaged for psilocybin and 98 dendrites from 3 *Thy1*^{GFP}*Htr2a*$^{f/f}$ mice were imaged for saline.

For calcium imaging of dendrites, the mouse was habituated to head fixation in an acrylic tube under the microscope for 3–4 days, with increasing durations each day, before the day of data collection. To examine the acute effects of psilocybin, we imaged 2 fields of view, each for 10 min to obtain pretreatment baseline data. Imaging was then paused to inject psilocybin (1 mg per kg, i.p.) or saline (10 ml per kg, i.p.). At 30 min after injection, we imaged those same two fields of view again, each for 10 min to acquire post-treatment data. Each animal received both psilocybin and saline, with at least 1 week between imaging sessions and the order of treatment was balanced across subjects, except for two IT mice that were administered only saline and psilocybin separately. For calcium imaging of dendrites, 8 C57BL/6J mice, including 3 male and 5 female mice, were treated with psilocybin (244 dendritic branches, including 149 from PT and 95 from IT neurons; with 4,835 dendritic spines, including 2,637 from PT and 2,198 from IT neurons) and saline (230 dendritic branches, including 140 from PT and 90 from IT neurons; with 4,544 dendritic spines, including 2,307 from PT and 2,237 from IT neurons).

Analysis of the imaging data

For structural imaging of dendrites, motion correction was performed using StackReg plug-in[63] in ImageJ. Quantification of structural parameters, such as spine head width and spine protrusion length, were done according to standardized critera[64]. In brief, a dendritic spine was counted when the protrusion extended for >0.4 μm from the dendritic shaft. The line segment tool in ImageJ was used to measure the distances. The spine head width was determined as the width of the widest part of the spine head. Dendritic spine protrusion length referred to the distance from the tip of the head to the base at the shaft. Alterations in spine density, spine head width and spine protrusion length were calculated as the fold change compared with the value measured for each dendritic segment on the first imaging session (day −3). The raw values for spine

density, spine head width and spine protrusion length are provided in Extended Data Figs. 2c,d,g,h,u,v and 10g. The spine-formation rate was calculated by determining the number of newly formed dendritic spines between two consecutive imaging sessions (that is, day −3 and day −1) divided by the total number of dendritic spines counted in the preceding imaging session (that is, day −3). Similarly, the spine elimination rate was calculated by determining the number of missing dendritic spines between two consecutive imaging sessions divided by the total number of dendritic spines counted in the preceding imaging session. To assess the longitudinal alterations in spine formation and elimination rates, we calculated the difference of the spine formation or elimination rate from the baseline rate, which was the spine formation or elimination rate for same dendritic segment before psilocybin and saline injection (between day −3 and day −1). The raw values for spine formation and elimination rates are provided in Extended Data Figs. 2e,f,i,j and 10h. To divide IT neurons on the basis of laminar position, we treated those with cell bodies residing at a depth of between 200 and 400 μm below the dura as layer 2/3, and those with cell bodies residing at a depth between 450 μm and 650 μm as layer 5 (refs. 65,66).

For calcium imaging of dendrites, multi-page.tiff image files from one experiment were concatenated and processed with NoRMCorre[67] in MATLAB to correct for non-rigid translational motion. As an overview, processing involved: (1) regions of interest (ROI) corresponding to dendritic branches and spines were manually traced using an in-house graphical user interface in MATLAB; (2) the average fluorescence trace from each ROI was then processed similar to previous work[38] to exclude background neuropil signal, and converted to fractional change in fluorescence ($\Delta F/F(t)$); (3) deconvolve the fluorescence trace into discrete calcium events. Details for each of these processing steps are described below.

Dendritic branch and spine ROIs were manually traced by scrolling through the imaging frames to find putative dendritic segments (that is, neurite segments with >10 spiny protrusions showing a correlated pattern of fluorescence transients). First, a given branch ROI would be traced around the dendritic shaft segment using a lasso drawing tool. Next, the putative dendritic spines for that branch segment were captured using a circle drawing tool (typically 0.8- to 1.2-μm-diameter ROIs). For each ROI, the pixel-wise average was calculated at each data frame to generate a fluorescence time course $F_{ROI}(t)$. As calcium imaging was performed on the same FOV before and after drug injections, a single ROI mask was used to extract calcium signals before and after treatment. All ROI selection was done blinded to treatment group.

Each ROI was then processed to reduce the contribution from background neuropil. Taking each ROI's area and considering a circle with an equivalent area with radius r, an ROI-specific neuropil mask was created as an annulus with inner radius $2r$ and outer radius $3r$ centred on the centroid of the ROI. Neuropil masks excluded pixels belonging to any other dendritic branch or spine ROI. To exclude neuropil mask pixels that may belong to unselected dendritic structures, we calculated the time-average signal for each pixel, taking the median among pixels in the mask. Pixels were excluded from the neuropil mask if their time-averaged signal was higher than the median. Finally, the remaining pixels in the neuropil mask were averaged per data frame to generate $F_{neuropil}(t)$. Each ROI had the fluorescence from its neuropil mask subtracted as follows:

$$F(t) = F_{ROI}(t) - c \times F_{neuropil}(t)$$

where the neuropil correction factor, c, was set to 0.4. Next, the fractional change in fluorescence $\Delta F/F(t)$ was calculated for each ROI by normalizing $F(t)$ to its baseline, $F_0(t)$, estimated as the 10th percentile within a 2-min sliding window:

$$\Delta F/F(t) = (F(t) - F_0(t))/F_0(t)$$

For each dendritic spine's $\Delta F/F_{spine}(t)$, we estimated the branch-independent spine activity, $\Delta F/F_{synaptic}(t)$, by subtracting a scaled version of the fluorescence from the corresponding dendritic branch, $\Delta F/F_{branch}(t)$, as follows:

$$\Delta F/F_{synaptic}(t) = \Delta F/F_{spine}(t) - \alpha \times \Delta F/F_{branch}(t)$$

where the branch scaling factor, α, was computed in an ROI-specific manner using a linear regression of $\Delta F/F_{synaptic}(t)$ predicted by $\Delta F/F_{branch}(t)$ forced through the origin. In a previous study, we have calibration to show that, with this analysis approach, the majority of the spontaneously occurring calcium transients in dendritic spines can be attributed to synaptic activation[68].

Calcium events were detected using automated procedure for each $\Delta F/F_{spine}(t)$ and $\Delta F/F_{branch}(t)$ using a deconvolution peeling algorithm[69]. The peeling algorithm uses an iterative template-matching procedure to decompose a $\Delta F/F(t)$ trace into a series of elementary calcium events. The template for elementary calcium events was set to have an instantaneous onset, an amplitude of 0.3 and a single-exponential decay time constant of 1 s. In brief, the algorithm searches a given $\Delta F/F(t)$ trace for a match to the template calcium event, subtracts it from the trace (that is, peeling) and successively repeats the matching process until no events are found. This event detection process outputs the recorded event times with a temporal resolution by the original imaging frame rate. In this way, it is possible to detect multiple calcium events during the same imaging frame (for example, for large amplitude transients). For each imaging session, an ROI's calcium event rate was computed by dividing the number of calcium events by the duration of the imaging session. The calcium events were examined further by their binned amplitude (average number of calcium events per frame, among frames with at least one event detected) and frequency (number of imaging frames with at least one event, divided by the total imaging duration). The change in calcium event rate, amplitude and frequency across treatment injections was computed for each ROI using the post-injection minus pre-injection values divided by the pre-injection values and provided raw values for calcium event rates averaged across dendritic branches in the same FOV. Separately, we have tried analysing the $\Delta F/F_{spine}(t)$ and $\Delta F/F_{branch}(t)$ using a different calcium event detection algorithm OASIS[37], which yielded qualitatively similar results (data not shown).

Confocal imaging

After longitudinal two-photon imaging and at 3 days after psilocybin (1 mg per kg, i.p.) or saline (10 ml per kg, i.p.) injection, the mouse was deeply anaesthetized with isoflurane and transcardially perfused with PBS followed by PFA (4% in PBS). The brains were fixed in 4% PFA for 24 h at 4 °C, and then 50-μm-thick coronal brain slices were sectioned using a vibratome (VT1000S, Leica) and placed onto slides with a coverslip with mounting medium (Vector Laboratories, H-1500-10). The brain slices were imaged with a confocal microscope (LSM 710, Zeiss) equipped with a Plan-Apochromat ×63/1.40 NA oil objective (zoom 2.5) and 0.37-μm steps at 1,024 × 1,024 pixels with a resolution of 0.08 μm per pixel to collect the structural imaging data. In total, 204 dendrites from 10 mice were imaged for psilocybin (5 *Htr2a*$^{f/f}$ mice; 5 C57BL/6J mice), and 207 dendrites from 10 mice were imaged for saline (3 *Htr2a*$^{f/f}$ mice; 7 C57BL/6J mice).

Overview of behavioural studies

All behavioural assays were conducted between 10:00 and 16:00. For the animals used in chemogenetic manipulation, the same mice were tested on all assays. At least 2 weeks were allotted between stress-related assays. Mice were randomized into different groupings for each assay (that is, the same mouse could be part of the psilocybin group on first assay, and then saline group on the second assay).

For studies involving PT neurons, *Fezf2-2A-creER* mice were tested on fear extinction; then, 2–3 weeks after the last extinction session, on learned helplessness; then, 1–2 weeks later, on head-twitch response; and, finally, 3 weeks later, on tail suspension. We started,

for fear extinction, with 58 *Fezf2-2A-creER* mice injected with DREADD or control viruses, including 17 mice for psilocybin + mCherry (9 male, 8 female), 13 mice for saline + mCherry (7 male, 6 female), 13 mice for psilocybin + hM4DGi (8 male, 5 female) and 15 mice for saline + hM4DGi (7 male, 8 female). For learned helplessness, we had 57 *Fezf2-2A-creER* mice remaining, including 13 mice for psilocybin + mCherry (8 male, 5 female), 15 mice for saline + mCherry (8 male, 7 female), 16 mice for psilocybin + hM4DGi (9 male, 7 female) and 13 mice for saline + hM4DGi (5 male, 8 female). For head-twitch response, we had 53 *Fezf2-2A-creER* mice remaining, 9 mice were tested on both psilocybin and saline with 1-week interval while the rest received psilocybin or saline, including 14 mice for psilocybin + mCherry (6 male, 8 female), 13 mice for saline + mCherry (6 male, 7 female), 20 mice for psilocybin + hM4DGi (12 male, 8 female) and 15 mice for saline + hM4DGi (7 male, 8 female). For the tail-suspension test, we had 49 *Fezf2-2A-creER* mice remaining, including 14 mice for psilocybin + mCherry (7 male, 7 female), 10 mice for saline + mCherry (5 male, 5 female), 13 mice for psilocybin + hM4DGi (6 male, 7 female) and 12 mice for saline + hM4DGi (8 male, 4 female).

For studies involving IT neurons, *Plxnd1-2A-creER* mice were tested on learned helplessness, then 1–2 weeks later on head-twitch response and, finally, 3 weeks later on tail suspension. We started, for learned helplessness, with 47 *Plxnd1-2A-creER* mice injected with DREADD or control viruses, including 14 mice for psilocybin + mCherry (7 male, 7 female), 11 mice for saline + mCherry (5 male and 6 female), 11 mice for psilocybin + hM4DGi (6 male, 5 female) and 11 mice for saline + hM4DGi (5 male, 6 female). For head-twitch response, we had 47 *Plxnd1-2A-creER* mice remaining, 4 mice were tested on both psilocybin and saline with a 1-week interval while the rest received psilocybin or saline, including 15 mice for psilocybin + mCherry (8 male, 7 female), 12 mice for saline + mCherry (6 male, 6 female), 11 mice for psilocybin + hM4DGi (6 male, 5 female) and 13 mice for saline + hM4DGi (7 male, 6 female). For the tail-suspension test, we had 41 *Plxnd1-2A-creER* mice remaining, including 14 mice for psilocybin + mCherry (7 male, 7 female), 9 mice for saline + mCherry (5 male, 4 female), 9 mice for psilocybin + hM4DGi (5 male, 4 female) and 9 mice for saline + hM4DGi (5 male, 4 female).

For behavioural studies involving *Htr2a*$^{f/f}$ mice, separate groups of mice were used for each behavioural test. For learned helplessness, 16 local 5-HT$_{2A}$-receptor-knockout mice were tested: 8 mice with saline (4 male, 4 female) and 8 with psilocybin (4 male, 4 female). 24 littermates injected with control virus were tested: 13 with saline (6 male, 7 female) and 11 with psilocybin (6 male, 5 female). For the tail-suspension test, 17 local 5-HT$_{2A}$-receptor-knockout mice were tested: 9 mice with saline (5 male, 4 female) and 8 with psilocybin (4 male, 4 female). 18 littermates injected with control virus were tested: 9 mice with saline (5 male, 4 female) and 9 with psilocybin (5 male, 4 female). For head-twitch response, 15 local 5-HT$_{2A}$-receptor-knockout mice were tested: 8 mice with saline (4 male, 4 female) and 7 mice with psilocybin (3 male, 4 female). 15 littermate controls were tested: 6 with saline (3 male, 3 female) and 9 mice with psilocybin (4 male, 5 female). For head-twitch response involving *Camk2a*^{cre} mice, 12 *Camk2a*^{cre}*Htr2a*$^{f/f}$ mice (4 male, 8 female) and 11 littermate controls (3 male, 8 female) were tested with psilocybin.

Head-twitch response

For each mouse, DCZ (0.1 mg per kg, i.p.; HY-42110, MedChemExpress) or saline (10 ml per kg, i.p.) was injected if chemogenetic manipulation was tested, and then psilocybin (1 mg per kg, i.p.) or saline (10 ml per kg, i.p.) was injected 15 min later. Head-twitch response was measured in groups of 2–3 mice, typically with psilocybin- and saline-treated mice tested simultaneously. After the injection, each mouse was immediately placed into its own plexiglass chamber (4 in × 4 in × 4 in), which had a transparent lid and was positioned within a sound attenuating cubicle (Med Associates). A high-speed video camera (acA1920, Basler) was mounted overhead above the chambers. We recorded videos for 10 min. Between measurements, the chambers were thoroughly cleaned with 70% ethanol. The videos were scored for head twitches by a different experimenter blinded to the experimental conditions. Previously, we showed that head twitches can be quantified using magnetic ear tags[18]; however, here we were concerned that the ear tag might interfere with the performance in other behavioural assays so we opted for video recording.

Learned helplessness

For learned helplessness, we performed the assay using an active avoidance box with a stainless-steel grid floor and a shuttle box auto door separating the two compartments (8 in × 8 in × 6.29 in) inside a sound-attenuating cubicle (MED-APA-D1M, Med Associates). On day 1 and day 2, there was one induction session on each day. Each session consisted of 360 inescapable foot shocks delivered at 0.2 mA for 1–3 s, with a random inter-trial interval ranging from 1 to 15 s. At 10–15 min after the end of the second induction session, DCZ (0.1 mg per kg, i.p.) or saline (10 ml per kg, i.p.) was given (the animals used in chemogenetic manipulation), and then psilocybin (1 mg per kg, i.p.) or saline (10 ml per kg, i.p.) was injected 15 min later. On day 3, one test session was conducted, consisting of 30 escapable foot shocks delivered at 0.2 mA for 10 s, with an inter-trial interval of 30 s. A shock would be terminated early if the mouse moved to the other compartment. Movement of the mouse was captured by beam breaks in the shuttle box. A failure was counted when the mouse failed to escape before the end of a shock. After each induction or testing session, the shuttle box was cleaned with 70% ethanol. Before each testing session, the shuttle box was cleaned with 1% acetic acid solution to provide a different olfactory context.

Tail-suspension test

Animals were tested 24 h after administration of psilocybin (0.1 mg per kg i.p) or saline (10 ml per kg, i.p.). For chemogenetic manipulation, DCZ (0.1 mg per kg, i.p.) or saline (10 per kg, i.p.) was given 15 min before psilocybin or saline administration. Within a tall sound-attenuating cubicle (Med Associates), the setup included a metal bar elevated 30 cm from the floor. An animal was suspended from the metal bar by securing its tail to the bar using removable tape (NC9972972, Thermo Fisher Scientific). A small plastic tube was placed around the base of the tail to prevent tail climbing during the session. Videos of the suspended animals were recorded for 6 min. The behavioural apparatus was thoroughly cleaned with 70% ethanol before and after each session.

Stress-induced resistance to fear extinction

For chronic restraint stress, we based the procedures on a published study[70]. The mice were restrained inside a cone-shaped plastic bag with openings on both ends (Decapicone, MDC200, Braintree Scientific) for 3 h each day for 14 consecutive days. The opening corresponding to the rear of the mouse was sealed by tying a wire, leaving the mouse's tail protruding. Restrained animals were secured in an upright position inside an empty cage and monitored frequently. At 24 h after the end of last restraint session, we began fear conditioning and extinction procedures, which were performed using a near-infrared video fear conditioning system (MED-VFC2-SCT-M, Med Associates). Before each session, the mouse was brought to the behaviour room for habituation for around 30 min. The fear conditioning system was equipped with stainless-steel grid floor and was controlled by the VideoFreeze software (Med Associates). On day 1 (fear conditioning), the chamber had blank straight walls and stainless-steel grid floor. Surfaces of the chamber were cleaned with 70% ethanol (context A). Each mouse was conditioned individually in a chamber and given 3 min to habituate. Subsequently, it received five presentations of an auditory tone as the conditioned stimulus (CS; 4 kHz, 80 dB, 30 s duration). Each CS co-terminated with a footshock as the unconditioned stimulus (US; 0.8 mA, 2 s duration). A 90-s intertrial interval separated the CS + US pairings. On day 3 (fear extinction 1), for each mouse, DCZ (0.1 mg per kg, i.p.) or saline (10 per kg, i.p.) was injected, and then psilocybin (1 mg per kg, i.p.) or saline (10 per kg, i.p.) was injected 15 min later. Then, 45 min later, we started

the test for fear extinction, while the drug was presumably still present in the brain. The chamber had two black IRT acrylic sheets inserted for a sloped roof and stainless-steel grid floor covered with a white smooth floor. Surfaces of the chamber were cleaned with 1% acetic acid (context B). Each mouse was tested individually in a chamber and given 3 min to habituate. Subsequently, it received 15 presentations of the CS without the US. A 15-s intertrial interval separated the CS presentations. On day 4 (retention 1), we repeated the test for fear extinction in context B. On day 17 (retention 2), we repeated the test for fear extinction in context B.

In vivo electrophysiology

Mice were habituated to head fixation with increasing duration over several days. At least 3 h before recording, mice were anaesthetized with isoflurane and a 2-mm-diameter craniotomy was made over the medial frontal cortex (AP, 1.7 mm; ML, 0.5 mm). Cold (4 °C) aCSF was used to irrigate to clear debris and reduce heating during drilling. Care was taken to minimize bleeding and keep the area clear of bone fragments. The dura was removed using a metal pin (10130-10, Fine Science Tools). A piece of Surgifoam (1972, Johnson & Johnson) soaked in aCSF was placed above the brain tissue, which was covered with silicon polymer (0318, Smooth-On) to keep the craniotomy moist and clean before recording. For drug administration, to avoid inserting a needle during recording session, which we found to cause the animal to move and therefore compromise recording stability, we used a catheter system described previously[71]. A 22-gauge intravenous catheter system (B383323, BD Saf-T-Intima Closed IV Catheter Systems) was preloaded with psilocybin or saline and maintained at a neutral pressure. At 1 h before recording, the mice were briefly anaesthetized with isoflurane and implanted with the intravenous catheter to their intraperitoneal cavity and the catheter was fixed with a drop of Vetbond tissue adhesive (1469, 3M Vetbond). The mice were then head fixed and the catheter tubing was secured to the mouse holder acrylic tube with tape. Silicon polymer and Surgifoam were removed from the skull and the craniotomy was briefly irrigated with aCSF. A high-density silicon probe (Neuropixels 1.0, IMEC) with the ground and reference shorted was coated using a 10 µl drop of CM-DiI (1 mM in ethanol; C7000, Invitrogen). The probe was then slowly lowered (100 µm min^{-1}) into the brain using a micromanipulator (MPM; M3-LS-3.4-15-XYZ-MPM-Inverted, New Scale Technologies) to the target depth of ~2,000 µm. The probe was configured to record from 384 sites. At the target depth, we waited for the probe to settle for at least 30 min before recording began. Data were acquired using the OpenEphys software[72] in external reference mode. Action potential and local field potentials were recorded at 30 kHz and 2.5 kHz, respectively. Once the recording began, 30 min of baseline activity was collected. The animal was then administered either psilocybin or saline through the catheter and an additional 60 min of data were collected. At the end of each recording session, opto-tagging was performed to identify ChR2-expressing PT or IT neurons. A fibre-coupled 473 nm laser (Obis FP 473LX, Coherent) was connected to a 200 µm optical fibre, which was mounted onto the manipulator with an unjacketed end aimed at the craniotomy. The OpenEphys software was used to trigger a Pulse-Pal (1102, Sanworks) to drive the laser control unit to produce 20 ms pulses at 1 Hz and ~25 mW mm^{-2} per trial. Each trial lasts for 1 s, with an inter-trial interval of 980 s, and we conducted at least 500 trials.

For *Fezf2-2A-creER* mice treated with saline, we recorded from 551 cells from 6 animals (1 male, 5 female), including 104 tagged neurons and 447 untagged other single units. For *Fezf2-2A-creER* mice treated with psilocybin, we recorded from 439 cells from 5 animals (4 male, 1 female), including 70 tagged neurons and 369 untagged other single units. For *Plxnd1-2A-creER* mice treated with saline, we recorded from 701 cells from 5 animals (4 male, 1 female), including 38 tagged neurons and 663 untagged other single units. For *Plxnd1-2A-creER* mice treated with psilocybin, we recorded from 607 cells from 5 animals (4 male, 1 female), including 57 tagged neurons and 550 untagged other single units.

Analysis of in vivo electrophysiology data

SpikeInterface[73] was used to preprocess, spike sort and calculate single-unit metrics. Putative single units were initially identified by Kilosort (v.2.5)[74] and were further manually curated in Phy (https://github.com/kwikteam/phy). Phy was executed using a dedicated Python environment created with Miniconda. Quality and waveform metrics were generated via SpikeInterface. We included units that satisfied all the following quality metrics: present for at least 90% of the recording (presence ratio), ISI violation rate less than 0.5 and amplitude cut-off of less than 0.1. To identify opto-tagged neurons, we created peri-stimulus time histograms by aligning putative single-unit spiking activity to the onset of laser stimulation. We classified opto-tagged neurons by visual inspection, considering the latency to spike and reliability of spiking in response to onset of laser stimulation.

Analysis of single-cell transcriptomics data

We accessed the 'whole cortex and hippocampus 2020' SmartSeq single-cell RNA-seq dataset made publicly available by the Allen Institute[46] (https://doi.org/10.1016/j.cell.2021.04.021). We analysed cells that belong to neuron classes already identified by the Allen Institute as layer 2/3 (L2/3) IT, layer 4/5 IT, L5 IT, L6 IT, L5 PT and L6 CT. We restricted our analyses to cells that reside in frontal cortical regions: ACA, ALM, ORB and PL-ILA. This yielded 1,403 L2/3 IT, 3,118 L4/5 IT, 1,541 L5 IT, 640 L6 IT, 471 L5 PT and 2,159 L6 CT neurons. We extracted expression levels for 6 genes: *Htr1a*, *Htr2a*, *Htr2b* and *Htr2c*, which encode the 5-HT_{1A}, 5-HT_{2A}, 5-HT_{2B} and 5-HT_{2C} receptors, as well as *Slc17a7* and *Gad1*, which are markers for glutamatergic and GABAergic neurons. The expression level was quantified by calculating the trimmed mean (25–75%) of $\log_2(CPM + 1)$, where CPM is counts per million.

RNA isolation and RT–qPCR

Tissue around viral injection sites in the medial frontal cortex was microdissected with tools treated with RNase Away (7002, Thermo Fisher Scientific) and processed using a Dounce homogenizer in BrainBits Hibernate A (NC1787837, Thermo Fisher Scientific). The cell solution was layered onto OptiPrep Density Gradient Medium (D1556, Sigma-Aldrich) and centrifuged for lipid/myelin debris removal. Cell solution was filtered and GFP^+ cells were sorted (BD FACSMelody Cell Sorter). RNA was extracted from GFP^+ cells using the RNeasy Plus Mini Kit (74134, Qiagen). RNA was reverse transcribed to cDNA using the High Capacity cDNA Reverse Transcription Kit (4368814, Applied Biosystems), amplified with the KAPA SYBR FAST qPCR Master Mix (KK4603, Roche) using qPCR (QuantStudio 7 Pro) and normalized on the basis of reference gene *Gapdh* expression. Primers were designed using Primer3 and data were analysed using the comparative threshold cycle method. Some steps for studies involving $Camk2a^{cre}$ mice were different: tissue around the medial frontal cortex was processed using a Dounce homogenizer in TRIzol (Thermo Fisher Scientific, A33251). Homogenized solution was phase separated with chloroform (Electron Microscopy Sciences, 12540). RNA was precipitated with isopropyl alcohol (American Bio, AB07015-0100), washed with 75% ethanol and reconstituted in ultrapure distilled H_2O (Invitrogen 10977-015). RNA was reverse transcribed, amplified and analysed as above.

Slice electrophysiology

Brain slices were prepared as previously described[75]. In brief, mice were first anaesthetized with chloral hydrate (400 mg per kg, i.p.). After decapitation, the brains were removed rapidly and placed in ice-cold (around 4 °C) aCSF in which sucrose (252 mM) was substituted for NaCl (sucrose-ACSF) to prevent cell swelling. Coronal slices (300 µm) were cut in sucrose-ACSF with an oscillating-blade vibratome (VT1000S, Leica). Slices were allowed to recover for around 1–2 h in sucrose-ACSF before commencement of recording. The slices were then placed into a submerged recording chamber in standard ACSF, and the bath

temperature was raised to 32 °C. The standard ACSF (pH of around 7.35) was equilibrated with 95% O_2/5% CO_2 and contained 128 mM NaCl, 3 mM KCl, 2 mM $CaCl_2$, 2 mM $MgSO_4$, 24 mM $NaHCO_3$, 1.25 mM NaH_2PO_4 and 10 mM D-glucose. L5 pyramidal cells in the medial frontal cortex were visualized under an Olympus BX51WI microscope using a ×60 infrared objective with infrared differential interference contrast videomicroscopy. A digital CMOS camera (ORCA-spark, Hamamatsu) was used to visualize neurons in the slice. Low-resistance patch pipettes (3–5 MΩ) were pulled from borosilicate glass (Warner Instrument) using a horizontal micropipette puller (P-1000, Sutter Instrument). Pipettes were filled with internal solution containing 115 mM K-gluconate, 5 mM KCl, 2 mM $MgCl_2$, 2 mM Mg-ATP, 2 mM Na_2ATP, 10 mM Na_2-phosphocreatine, 0.4 mM Na_2GTP and 10 mM HEPES, calibrated to pH 7.33. Whole-cell patch clamp recording was performed with a Multiclamp 700B amplifier (Axon Instruments). The output signal was low-pass-filtered at 3 kHz, amplified 100× and digitized at 15 kHz and acquired using the Clampex 10.5/Digidata 1550A software. Series resistance, monitored throughout the experiment, was between 4–8 MΩ. Cells were discarded if the series resistance rose above 8 MΩ. Liquid junction potential was not corrected. sEPSCs were recorded by clamping cells near their resting potential (around −75 mV ± 5 mV) to minimize holding currents. After baseline recording, 20 μM 5-hydroxytryptamine creatinine sulfate (Sigma-Aldrich) was washed on for 2 min for recording in 5-HT. Subsequently, there was a washout, before 30 nM MDL100907 (Marion Merrell Dow) was washed on for 5 min and then recordings were made in 20 μM 5-HT + 30 nM MDL100907.

Analysis of sEPSC frequency was conducted using commercially available Mini Analysis software (Synaptosoft, Decatur). sEPSCs were detected and measured according to the amplitude, rise time, duration and area under the curve (fc). Synaptic events were those with an amplitude threshold of 5 pA and area threshold of 50 fc. Traces were recorded for 60 s, and the average of three traces (180 s) was used for analysis for each cell/treatment.

For local 5-HT_{2A}-receptor-knockout mice, we recorded from 23 cells from 4 animals for the baseline, continued to obtain recording from the same 23 cells after bath application of 20 μM 5-HT and, for 7 of the cells, recorded after bath application of 20 μM 5-HT and 100 nM MDL100907. For the *Htr2a*$^{f/f}$ mice injected with control virus, we recorded from 22 cells from 4 animals for the baseline, continued to obtain recording from the same 22 cells after bath application of 20 μM 5-HT and, for 6 of the cells, recorded after bath application of 20 μM 5-HT and 100 nM MDL100907. Some cells did not go through all treatment conditions, because the seal had degraded and the input resistance changed significantly.

Immunohistochemistry

Brains were sectioned using a vibratome (VT1000S, Leica) to yield 50-μm-thick coronal sections. The free-floating sections were washed three times with 0.3% Triton X-100/PBS before a 1-h incubation in blocking buffer (5% normal donkey serum in 0.3% Triton X-100/PBS) and then incubated overnight at room temperature with anti-rabbit HTR2A antibody (1:250, RA24288, Neuromics). The brain sections were washed with 0.3% Triton X-100/PBS three times and then incubated with goat anti-rabbit IgG AlexaFluor 555 (1:1,000 dilution, A21528, Invitrogen) secondary antibodies at room temperature for 2 h. The sections were washed three times with PBS. The sections were mounted and coverslipped with Vectashield Mounting Medium with DAPI (H-1500-10, Vector Laboratories). Tissue sections were imaged on a Zeiss LSM 710 Confocal Microscope with a Plan-Apochromat ×63/1.40 NA oil objective.

Statistics and reproducibility

Supplementary Table 1 provides detailed information about the sample sizes and statistical analyses for each experiment. Sample sizes were based on pilot and existing relevant studies and were not statistically predetermined. All tests were two-sided, and results are displayed as the mean ± s.e.m. For behavioural studies and confocal imaging, statistical analyses were performed with GraphPad Prism 10. For two-photon imaging experiments, statistical analyses were performed on the basis of mixed-effects models using the lme4 package in R. Linear mixed-effects models were used to account for repeated measures and within-subject nesting (for example, multiple spines per branch) in a manner that makes less assumptions about underlying data than the commonly used repeated-measures ANOVA. Details about the models are described below.

For two-photon imaging of dendritic structure, analyses were performed blinded to treatment and cell type or genotype. A separate mixed-effects model was constructed for each of five dependent variables related to dendritic spines: spine density, average spine head width, spine protrusion length, spine-formation rate and spine elimination rate. Each model included fixed-effects terms for treatment (psilocybin versus saline), cell type (PT versus IT), sex (female versus male) and time (day 1 to day 65) as factors, in addition to all second- and higher-order interactions among these terms. The variation for repeated measures within mouse, cell and dendrite were accounted for by including a random intercept for dendrites nested by cell nested by mice. Residuals plots were inspected visually to confirm no deviations from homoscedasticity or normality. Fixed-effect *P* values were computed using likelihood ratio tests comparing the full model against a model without the effect in question. Post-hoc two-sample *t*-tests were used to contrast psilocybin and saline groups per day, with and without splitting the sample by sex. The *P* values resulting from post-hoc *t*-tests were Bonferroni corrected for multiple comparisons. For two-photon imaging involving *Htr2a*$^{f/f}$ mice, a similar mixed-effects model and post-hoc *t*-tests were used, except each model included fixed-effects terms for treatment (psilocybin versus saline), genotype (*Htr2a*$^{f/f}$ versus wild type) and time (day 1 and day 3) as factors, in addition to all second- and higher-order interactions among these terms. For two-photon imaging involving *Thy1*^{GFP}*Htr2a*$^{f/f}$ mice, two-factor ANOVA was used for the analyses of spine density to test the interaction between treatment (psilocybin versus saline) and conditions (*Thy1*^{GFP} *Htr2a*$^{+/+}$ + psilocybin versus *Thy1*^{GFP}*Htr2a*$^{f/f}$ + psilocybin versus *Thy1*^{GFP}*Htr2a*$^{f/f}$ + saline) and time (day 1 to day 7). Post-hoc *t*-tests were used to compare *Thy1*^{GFP}*Htr2a*$^{+/+}$ + psilocybin versus *Thy1*^{GFP}*Htr2a*$^{f/f}$ + psilocybin, *Thy1*^{GFP}*Htr2a*$^{f/f}$ + psilocybin versus *Thy1*^{GFP}*Htr2a*$^{f/f}$ + saline or *Thy1*^{GFP}*Htr2a*$^{+/+}$ + psilocybin and *Thy1*^{GFP}*Htr2a*$^{f/f}$ + saline. Bonferroni correction was used for multiple comparisons. Fold changes in spine density, spine head width and spine protrusion length, and the difference in spine-formation rate and spine elimination rate were shown as percentages for visualization purposes. For statistical analysis, original fold change values were used.

For imaging of dendritic calcium signals, blinding procedures were implemented by having one person perform the imaging and scramble the group names, and another person analysed the data blinded to treatment and cell type information. Data were unblinded after all of the analyses were completed. A similar linear mixed-effects modelling approach was used to examine three dependent variables: calcium event rate, amplitude and frequency. Dendritic branch and spine (branch independent) signals were analysed in separate models (that is, six models total). Each model included fixed-effects terms for treatment (psilocybin versus saline), cell type (PT versus IT) and the interaction term for treatment × cell type. Treatment order (psilocybin before saline versus psilocybin after saline) was included in the model as a nuisance variable. The variation for repeated measures of mice and dendrites was accounted for by including a random intercept for dendrites nested by FOV nested by mice. Post-hoc two-sample *t*-tests were used to contrast psilocybin and saline groups, with and without splitting the sample by cell type. The calcium imaging statistical outputs were processed akin to the structural imaging model outputs as described above (that is, residuals plots were inspected, fixed-effect *P* values were computed with likelihood ratio tests, and post-hoc two-sample *t*-test *P* values were Bonferroni-corrected for multiple comparisons).

For confocal imaging, two-factor ANOVA was used for the analyses of spine density, spine head width and spine protrusion length to test the interaction between treatment (psilocybin versus saline) and genotype (*Htr2a*$^{f/f}$ versus wild type). Post-hoc *t*-tests were used to compare psilocybin + PT neuron-targeted 5-HT$_{2A}$ receptor knockout versus saline + PT neuron-targeted 5-HT$_{2A}$ receptor knockout, or psilocybin + wild-type and saline + wild-type. Bonferroni correction was used for multiple comparisons.

For behavioural studies, performance was analysed using software with automated procedures for fear extinction and learned helplessness. For head-twitch response and tail-suspension tests, video scoring was done by a different experimenter blinded to conditions. For PT/IT studies, Two-factor ANOVA and post-hoc *t*-tests were used for head-twitch response, learned-helplessness and tail-suspension tests. The same statistical test was used for fear conditioning, extinction and retention to test the interaction between treatment (psilocybin versus saline) and DREADD (hM4DGi versus mCherry). Post-hoc *t*-tests were used to compare psilocybin + mCherry versus saline + mCherry or psilocybin + hM4DGi and saline + hM4DGi for different sets of tones in a session. Bonferroni correction was applied for multiple comparisons. Owing to a technical issue (faulty USB connection causing VideoFreeze software to crash in the middle of a session), a small subset of data from some mice was not used for the statistical test. For behavioural studies involving *Htr2a*$^{f/f}$ mice, two-tailed unpaired *t*-tests were used to compare control + saline versus control + psilocybin and local 5-HT$_{2A}$ receptor knockout + saline versus local 5-HT$_{2A}$ receptor knockout + psilocybin. For head-twitch response involving in *Camk2a*^{cre}*Htr2a*$^{f/f}$ mice, two-tailed unpaired *t*-tests were used to compare *Camk2a*^{cre}*Htr2a*$^{f/f}$ versus control mice. For slice electrophysiology, two-tailed unpaired *t*-tests were used to compare control baseline versus control with 5HT; KO baseline versus KO with 5HT; control baseline versus control with 5HT + MDL; or KO baseline versus KO with 5HT + MDL.

For in vivo electrophysiology, we first identified opto-tagged neurons by constructing 0.1 ms bin peristimulus time histogram plots aligned to the laser pulse onset. For comparison of time to first spike latency between PT and IT neurons, we conducted two-sided two-sample Kolmogorov–Smirnov tests of time to first spike for all neurons. To compare the baseline firing rates we used a two-sample independent *t*-test. For comparing the changes in firing rates before and after administration of saline or psilocybin, we conducted a paired two-sided *t*-test using each neuron's baseline mean firing rate in the 30-min period before saline or drug administration and the mean firing rate in the 60-min period after saline or drug administration and Bonferroni correction was applied for *P* values.

Data were collected from multiple experiments. To ensure replicability of findings, all behavioural tests and in vivo electrophysiology recordings were performed in at least two cohorts, and data were combined and analysed together in a blinded manner. For imaging experiments, we used at least three biological (mice) replicates per experimental condition. All two-photon imaging experiments were conducted in at least three cohorts, with data combined and analysed together in a blinded manner. The exact sample sizes are provided in the Methods and the Supplementary Table 1. All attempts at replication were successful.

Reporting summary

Further information on research design is available in the Nature Portfolio Reporting Summary linked to this article.

Data availability

Details for sample sizes and statistical tests for all experiments are provided in Supplementary Table 1. Data associated with the study are available at GitHub (https://github.com/Kwan-Lab/shaoliao2025). The RNA-seq dataset was obtained from publicly available sources at the Allen Institute (https://doi.org/10.1016/j.cell.2021.04.021). Source data are provided with this paper.

Code availability

Code for data analysis associated with the study are available at GitHub (https://github.com/Kwan-Lab/shaoliao2025), and from the corresponding author on request.

57. Feng, G. et al. Imaging neuronal subsets in transgenic mice expressing multiple spectral variants of GFP. *Neuron* **28**, 41–51 (2000).
58. Tervo, D. G. et al. A designer AAV variant permits efficient retrograde access to projection. *Neuron* **92**, 372–382 (2016).
59. Shamash, P., Carandini, M., Harris, K. D. & Steinmetz, N. A. A tool for analyzing electrode tracks from slice histology. Preprint at *bioRxiv* https://doi.org/10.1101/447995 (2018).
60. Wang, Q. et al. The Allen Mouse Brain Common Coordinate Framework: a 3D reference atlas. *Cell* **181**, 936–953 (2020).
61. Claudi, F. et al. Visualizing anatomically registered data with brainrender. *eLife* **10**, e65751 (2021).
62. Pologruto, T. A., Sabatini, B. L. & Svoboda, K. ScanImage: flexible software for operating laser scanning microscopes. *Biomed. Eng. Online* **2**, 13 (2003).
63. Thevenaz, P., Ruttimann, U. E. & Unser, M. A pyramid approach to subpixel registration based on intensity. *IEEE Trans. Image Process.* **7**, 27–41 (1998).
64. Holtmaat, A. et al. Long-term, high-resolution imaging in the mouse neocortex through a chronic cranial window. *Nat. Protoc.* **4**, 1128–1144 (2009).
65. Mitrić, M. et al. Layer- and subregion-specific electrophysiological and morphological changes of the medial prefrontal cortex in a mouse model of neuropathic pain. *Sci. Rep.* **9**, 9479 (2019).
66. Radnikow, G. & Feldmeyer, D. Layer- and cell type-specific modulation of excitatory neuronal activity in the neocortex. *Front. Neuroanat.* **12**, 1 (2018).
67. Pnevmatikakis, E. A. & Giovannucci, A. NoRMCorre: an online algorithm for piecewise rigid motion correction of calcium imaging data. *J. Neurosci. Methods* **291**, 83–94 (2017).
68. Ali, F. et al. Inhibitory regulation of calcium transients in prefrontal dendritic spines is compromised by a nonsense *Shank3* mutation. *Mol. Psychiatry* **26**, 1945–1966 (2021).
69. Lutcke, H., Gerhard, F., Zenke, F., Gerstner, W. & Helmchen, F. Inference of neuronal network spike dynamics and topology from calcium imaging data. *Front. Neural Circuits* **7**, 201 (2013).
70. Friedman, A. et al. A corticostriatal path targeting striosomes controls decision-making under conflict. *Cell* **161**, 1320–1333 (2015).
71. Boudreau, E. et al. Intraperitoneal catheter placement for pharmacological imaging studies in conscious mice. *Lab. Anim.* **39**, 23–25 (2010).
72. Siegle, J. H. et al. Open Ephys: an open-source, plugin-based platform for multichannel electrophysiology. *J. Neural Eng.* **14**, 045003 (2017).
73. Buccino, A. P. et al. SpikeInterface, a unified framework for spike sorting. *eLife* **9**, e61834 (2020).
74. Pachitariu, M. et al. Kilosort: realtime spike-sorting for extracellular electrophysiology with hundreds of channels. Preprint at *bioRxiv* https://doi.org/10.1101/061481 (2016).
75. Liu, R. J. & Aghajanian, G. K. Stress blunts serotonin- and hypocretin-evoked EPSCs in prefrontal cortex: role of corticosterone-mediated apical dendritic atrophy. *Proc. Natl Acad. Sci. USA* **105**, 359–364 (2008).

Acknowledgements We thank L. Sun for help with analysing the slice electrophysiology data. Psilocybin was provided by Usona Institute's Investigational Drug & Material Supply Program. The Usona Institute IDMSP is supported by A. Sherwood, R. Kargbo and K. Kaylo. This work was supported by NIH grants R01MH121848, R01MH128217, R01MH137047, U01NS128660, One Mind–COMPASS Rising Star Award (A.C.K.); NIH training grants T32GM007205 (P.A.D. and N.K.S.), T32NS041228 (C.L.); NIH fellowships F30DA059437 (P.A.D.) and F30MH129085 (N.K.S.); Source Research Foundation student grant (P.A.D.); NIH instrumentation grants S10RR025502 and S10OD032251 (Cornell Biotechnology Resource Center Imaging Facility); NIH grants R00NS114166, R01NS133434 and R01DA059378 (A.C.); State of Connecticut, Department of Mental Health and Addiction Services (A.C. and R.-J.L.).

Author contributions L.-X.S., C.L. and A.C.K. planned the study. L.-X.S. and C.L. conducted and analysed the imaging and behavioural experiments. P.A.D. and Q.J. conducted and analysed the electrophysiological experiments. N.K.S. and O.M.B. analysed the dendritic calcium imaging data. R.-J.L. and A.C. conducted slice electrophysiology experiments. Q.J. assisted in animal surgery. Q.J., D.T., C.W. and J.D.N. assisted in behavioural experiments and histology. S.C.W. and C.W. conducted pilot studies to validate the protocols for the behavioural assays. H.K. generated and provided the *Htr2a*$^{f/f}$ mice. L.-X.S., C.L. and A.C.K. drafted the manuscript. All of the authors reviewed the manuscript before submission.

Competing interests A.C.K. has been a scientific advisor or consultant for Boehringer Ingelheim, Empyrean Neuroscience, Freedom Biosciences and Xylo Bio. A.C.K. has received research support from Intra-Cellular Therapies. The other authors declare no competing interests.

Additional information

Supplementary information The online version contains supplementary material available at https://doi.org/10.1038/s41586-025-08813-6.

Correspondence and requests for materials should be addressed to Alex C. Kwan.

Peer review information *Nature* thanks Adema Ribic, Bryan Roth and the other, anonymous, reviewer(s) for their contribution to the peer review of this work. Peer reviewer reports are available.